Robin Based Semi-Implicit Coupling in Fluid-Structure Interaction: Stability Analysis and Numerics

Matteo Astorino, Franz Chouly, Miguel Angel Fernández

INSTITUT NATIONAL DE RECHERCHE EN INFORMATIQUE ET EN AUTOMATIQUE

Robin Based Semi-Implicit Coupling in Fluid-Structure Interaction: Stability Analysis and Numerics

Matteo Astorino — Franz Chouly — Miguel A. Fernández

N° ????

February 2009

Thème BIO

ISSN 0249-6399 ISRN INRIA/RR--????--FR+ENG

Robin Based Semi-Implicit Coupling in Fluid-Structure Interaction: Stability Analysis and Numerics

Matteo Astorino* , Franz Chouly * , Miguel A. Fernández *†

Thème BIO — Systèmes biologiques
Projet REO

Rapport de recherche n° ???? — February 2009 — 30 pages

Abstract: In this report, we propose a semi-implicit coupling scheme for the numerical simulation of fluid-structure interaction systems involving a viscous incompressible fluid. The scheme is stable irrespectively of the so-called added-mass effect and allows for conservative time-stepping within the structure. The efficiency of the scheme is based on the explicit splitting of the viscous effects and geometrical/convective non-linearities, through the use of the Chorin-Temam projection scheme within the fluid. Stability comes from the implicit pressure-solid coupling and a specific Robin treatment of the explicit viscous-solid coupling, derived from Nitsche's method.

Key-words: Fluid-structure interaction, Chorin-Temam projection scheme, Robin interface conditions, Nitsche's method, fluid incompressibility, added-mass effect, time discretization, semi-implicit coupling, partitioned scheme.

Preprint submitted for publication to *SIAM Journal on Scientific Computing*

* INRIA, REO project-team
† Correspondence to: `miguel.fernandez@inria.fr`

Unité de recherche INRIA Rocquencourt
Domaine de Voluceau, Rocquencourt, BP 105, 78153 Le Chesnay Cedex (France)
Téléphone : +33 1 39 63 55 11 — Télécopie : +33 1 39 63 53 30

Résumé : Dans ce rapport, nous proposons un schéma de couplage semi-implicite pour la simulation numérique de problèmes d'interaction fluide-structure où intervient un fluide visqueux incompressible. Le schéma est stable indépendamment de l'effet de masse-ajoutée et permet d'utiliser une discrétisation conservative pour la structure. L'efficacité du schéma repose sur le découplage explicite des effets visqueux et non-linéaires (convection et géometrie), grâce au schéma de Chorin-Temam. La stabilité provient du couplage implicite solide-pression et d'un traitement spécifique du couplage explicite par des conditions de type Robin, dérivées à partir de la méthode de Nitsche.

Mots-clés : Interaction fluide-structure, méthode de projection de Chorin-Temam, conditions d'interface de type Robin, méthode de Nitsche, fluide incompressible, effet de masse-ajoutée, discrétisation en temps, couplage semi-implicite, schéma partitionné.

1 Introduction

In this paper, we address the numerical simulation of fluid-structure interaction problems involving a viscous incompressible fluid and an elastic structure. For this type of problems, it is well known that stability of conventional (*Dirichlet-to-Neumann* based) *explicit coupling* schemes, i.e. that only involve the solution of the fluid and the structure once (or just a few times) per time step, is dictated by the amount of *added-mass effect* (see e.g. [9]). In other words, a strong added-mass effect in the system (the fluid and solid densities are close or the domain is slender) gives rise to unconditional numerical instability, that is, irrespectively of the discretization parameters. Examples in blood flows simulations are popular.

Several strategies have been proposed in the literature in order to overcome these infamous numerical instabilities: *implicit coupling* (see e.g. [17, Chapter 9] for a review), *semi-implicit coupling* [13, 14, 27, 5, 30] or *stabilized explicit coupling* [7, 8]. Moreover, some explicit coupling procedures, based on the use of a simplified structural model, have been recently reported in [26, 21].

In the present work, we consider the original semi-implicit coupling approach reported in [13, 14]. Computational cost and numerical stability are then balanced by performing an explicit-implicit splitting, based on the use of the Chorin-Temam's projection scheme within the fluid [10, 31]. At each time step, the projection sub-step is implicitly coupled with the structure, whereas the viscous sub-step, taking into account the convective–viscous effects and the geometrical non-linearities, is treated explicitly.

Although the theoretical and numerical results, reported in [14], showed that the resulting algorithm drastically improves the stability properties of conventional explicit coupling and the efficiency of implicit coupling, the original semi-implicit coupling scheme has two limitations. On one hand, though much less sensitive to the added-mass effect than explicit coupling, numerical evidence (see section §5) shows that the stability still depends on the fluid-solid density ratio. As a matter of fact, in the linear case, stability is obtained (see [14, Theorem 1]) under a condition of the type:

$$\rho^{\mathrm{s}}/\rho^{\mathrm{f}} \geq C\left[1+\mu\tau/(\rho^{\mathrm{f}}h^2)\right], \tag{1}$$

where $\rho^{\mathrm{s}}, \rho^{\mathrm{f}}$ stand for the solid and fluid densities, μ for the fluid viscosity and h, τ for the space and time discretization parameters. On the other hand, from the theoretical point of view, a dissipative time-discretization is required within the structure in order to ensure stability (see [14, Remarks 3 and 4]).

In the present paper, we propose a semi-implicit coupling scheme that circumvents the above mentioned inconveniences. The stability properties of the new scheme are independent of the added-mass effect and allow for conservative time-stepping within the structure. The key idea consists in treating the explicit part of the coupling in a weak sense, by using a specific Robin coupling derived from Nitsche's interface method (see e.g. [6, 22, 7, 8]).

The remainder of the paper is organized as follows. The non-liner fluid-structure interaction problem, that aims to be solved, and its time discretization are described in section §2. The proposed Robin based semi-implicit coupling is detailed in section §3. Section §4 is devoted to the stability analysis. We show that the linearized version of the algorithm is stable (in the energy norm)

irrespectively of the added-mass effect and of the numerical dissipation within the structure. Numerical experiments, in two and three space dimensions, are carried out in section §5, illustrating the theoretical results. Finally, some concluding remarks are given in section §6.

Some preliminary results of this work have been announced, without proof, in [1].

2 Preliminaries

This section contains standard material (see e.g. [17, Chapters 3 and 9]). We introduce some notations and describe the non-linear coupled problem that models the mechanical interaction between a viscous incompressible fluid and an elastic structure. The resulting equations are semi-discretized in time using the semi-implicit coupling scheme introduced in [13, 14].

2.1 The Coupled Problem

We consider an ALE (Arbitrary Lagrangian Eulerian) formulation for the fluid and a total Lagrangian formulation for the solid (see e.g. [17, Chapter 3]).

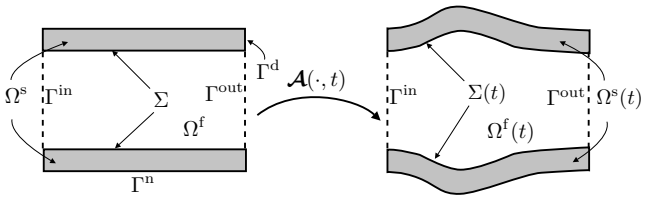

Figure 1: Geometrical description

Let $\Omega = \Omega^{\mathrm{f}} \cup \Omega^{\mathrm{s}}$ be a reference configuration of the fluid-structure system, we denote by $\Sigma \stackrel{\mathrm{def}}{=} \partial\Omega^{\mathrm{f}} \cap \partial\Omega^{\mathrm{s}}$ the fluid-solid interface and $\partial\Omega^{\mathrm{f}} = \Gamma^{\mathrm{in-out}} \cup \Sigma$, $\partial\Omega^{\mathrm{s}} = \Gamma^{\mathrm{d}} \cup \Gamma^{\mathrm{n}} \cup \Sigma$, are given partitions of the fluid and solid boundaries respectively, see Figure 1. The current configuration of the fluid domain, $\Omega^{\mathrm{f}}(t)$, is parametrized by the ALE map $\boldsymbol{\mathcal{A}} \stackrel{\mathrm{def}}{=} \boldsymbol{I}_{\Omega^{\mathrm{f}}} + \boldsymbol{d}^{\mathrm{f}}$ as $\Omega^{\mathrm{f}}(t) = \boldsymbol{\mathcal{A}}(\Omega^{\mathrm{f}}, t)$, where $\boldsymbol{d}^{\mathrm{f}} : \Omega^{\mathrm{f}} \times \mathbb{R}^+ \to \mathbb{R}^d$ ($d = 2, 3$) stands for the displacement of the fluid domain. We denote by $\Sigma(t) \stackrel{\mathrm{def}}{=} \partial\Omega^{\mathrm{s}}(t) \cap \partial\Omega^{\mathrm{f}}(t)$ the current position of the fluid-solid interface. In practice, $\boldsymbol{d}^{\mathrm{f}} = \mathrm{Ext}(\boldsymbol{d}|_{\Sigma})$, where $\boldsymbol{d} : \Omega^{\mathrm{s}} \times \mathbb{R}^+ \to \mathbb{R}^d$ is the solid displacement and $\mathrm{Ext}(\cdot)$ denotes a reasonable lifting operator from the (reference) interface Σ into the (reference) fluid domain Ω^{f} (e.g. an harmonic lifting operator).

The non-linear fluid-structure problem under consideration reads as follows (see e.g. [17, Chapter 3]):
Find the fluid velocity $\boldsymbol{u} : \Omega^{\mathrm{f}} \times \mathbb{R}^+ \to \mathbb{R}^d$, the pressure $p : \Omega^{\mathrm{f}} \times \mathbb{R}^+ \to \mathbb{R}$ and

the solid displacement $\boldsymbol{d} : \Omega^{\mathrm{s}} \times \mathbb{R}^+ \to \mathbb{R}^d$ such that

$$\begin{cases} \rho^{\mathrm{f}} \partial_t \boldsymbol{u}|_{\mathcal{A}} + \rho^{\mathrm{f}} (\boldsymbol{u} - \boldsymbol{w}) \cdot \boldsymbol{\nabla} \boldsymbol{u} - \boldsymbol{\nabla} \cdot \boldsymbol{\sigma}^{\mathrm{f}}(\boldsymbol{u}, p) = \boldsymbol{0} & \text{in} \quad \Omega^{\mathrm{f}}(t), \\ \boldsymbol{\nabla} \cdot \boldsymbol{u} = 0 & \text{in} \quad \Omega^{\mathrm{f}}(t), \\ \boldsymbol{\sigma}^{\mathrm{f}}(\boldsymbol{u}, p) \boldsymbol{n}^{\mathrm{f}} = -\bar{p} \boldsymbol{n}^{\mathrm{f}} & \text{on} \quad \Gamma^{\mathrm{in-out}}, \\ \rho^{\mathrm{s}} \partial_{tt} \boldsymbol{d} - \boldsymbol{\nabla} \cdot \boldsymbol{\Pi}(\boldsymbol{d}) = \boldsymbol{0} & \text{in} \quad \Omega^{\mathrm{s}}, \\ \boldsymbol{d} = \boldsymbol{0} & \text{on} \quad \Gamma^{\mathrm{d}}, \\ \boldsymbol{\Pi}(\boldsymbol{d}) \boldsymbol{n}^{\mathrm{s}} = \boldsymbol{0} & \text{on} \quad \Gamma^{\mathrm{n}}, \end{cases} \tag{2}$$

with the interface coupling conditions

$$\begin{cases} \boldsymbol{d}^{\mathrm{f}} = \mathrm{Ext}(\boldsymbol{d}|_{\Sigma}), \quad \boldsymbol{w} = \partial_t \boldsymbol{d}^{\mathrm{f}} \quad \text{in} \quad \Omega^{\mathrm{f}}, \quad \Omega^{\mathrm{f}}(t) = (\boldsymbol{I}_{\Omega^{\mathrm{f}}} + \boldsymbol{d}^{\mathrm{f}})(\Omega^{\mathrm{f}}), \\ \boldsymbol{u} = \partial_t \boldsymbol{d} \quad \text{on} \quad \Sigma(t), \\ \boldsymbol{\Pi}(\boldsymbol{d}) \boldsymbol{n}^{s} = -J^{\mathrm{f}} \boldsymbol{\sigma}^{\mathrm{f}}(\boldsymbol{u}, p) (\boldsymbol{F}^{\mathrm{f}})^{-\mathrm{T}} \boldsymbol{n}^{\mathrm{f}} \quad \text{on} \quad \Sigma. \end{cases} \tag{3}$$

The initial conditions are: $\boldsymbol{u}(0) = \boldsymbol{u}_0$, $\boldsymbol{d}(0) = \boldsymbol{d}_0$, $\partial_t \boldsymbol{d}(0) = \dot{\boldsymbol{d}}_0$; $\bar{p}$ is a given pressure at $\Gamma^{\mathrm{in-out}}$; ρ^{f} and ρ^{s} represent respectively the fluid and solid densities, $\partial_t|_{\mathcal{A}}$ the ALE time derivative, $\boldsymbol{\sigma}^{\mathrm{f}}(\boldsymbol{u}, p) \stackrel{\mathrm{def}}{=} -p\boldsymbol{I} + 2\mu \boldsymbol{\epsilon}(\boldsymbol{u})$ the fluid Cauchy stress tensor, μ the fluid dynamic viscosity, $\boldsymbol{\epsilon}(\boldsymbol{u}) \stackrel{\mathrm{def}}{=} \frac{1}{2} \left(\boldsymbol{\nabla} \boldsymbol{u} + \boldsymbol{\nabla} \boldsymbol{u}^{\mathrm{T}} \right)$ the strain rate tensor, $\boldsymbol{\Pi}(\boldsymbol{d})$ the first Piola-Kirchhoff stress tensor of the structure, $\boldsymbol{F}^{\mathrm{f}} \stackrel{\mathrm{def}}{=} \boldsymbol{\nabla} \mathcal{A}$ the fluid domain gradient of deformation and $J^{\mathrm{f}} \stackrel{\mathrm{def}}{=} \det \boldsymbol{F}^{\mathrm{f}}$ the Jacobian; $\boldsymbol{n}^{\mathrm{f}}$ and $\boldsymbol{n}^{\mathrm{s}}$ are the outward unit normals to the fluid and solid domains, respectively. Note that a field defined in the reference fluid domain, Ω^{f}, is evaluated in the current fluid domain, $\Omega^{\mathrm{f}}(t)$, by composition with $\mathcal{A}^{-1}(\cdot, t)$.

2.2 Time Semi-Discretization

We now propose to semi-discretize in time the non-linear coupled problem (2)-(3) using the framework of the semi-implicit coupling scheme introduced in [13]. The fluid equations $(2)_{1,2}$ are discretized in time using the projection Chorin-Temam's scheme, whereas for the structure $(2)_4$ we consider a conservative mid-point scheme. The time discretization of (3) is semi-implicit, that is, the fluid-domain geometry $(3)_1$, the viscous kinematic condition $(3)_2$ and the viscous stresses in $(3)_3$ are treated explicitly whereas the pressure stresses are implicitly coupled to the structure.

More precisely, denoting by τ the time-step length, by $D_\tau X^{n+1} \stackrel{\mathrm{def}}{=} (X^{n+1} - X^n)/\tau$ the first order backward difference in time and by $X^{n+\frac{1}{2}} \stackrel{\mathrm{def}}{=} (X^{n+1} + X^n)/2$ the mid-point value approximation, we consider the following semi-implicit time discretization of (2)-(3), see [13, 14]:

- Update fluid domain:

$$\begin{aligned} &\boldsymbol{d}^{\mathrm{f},n+1} = \mathrm{Ext}(\boldsymbol{d}^n|_{\Sigma}), \quad \boldsymbol{w}^{n+1} = D_\tau \boldsymbol{d}^{\mathrm{f},n+1} \quad \text{in} \quad \Omega^{\mathrm{f}}, \\ &\Omega^{\mathrm{f},n+1} = (\boldsymbol{I}_{\Omega^{\mathrm{f}}} + \boldsymbol{d}^{\mathrm{f},n+1})(\Omega^{\mathrm{f}}). \end{aligned} \tag{4}$$

- Implicit step (pressure-structure coupling):

– Fluid projection sub-step:

$$\begin{cases} \dfrac{\rho^{\mathrm{f}}}{\tau}\left(\boldsymbol{u}^{n+1}-\widetilde{\boldsymbol{u}}^{n}\right)+\boldsymbol{\nabla}p^{n+1}=0 & \text{in} \quad \Omega^{\mathrm{f},n}, \\ \boldsymbol{\nabla}\cdot\boldsymbol{u}^{n+1}=0 & \text{in} \quad \Omega^{\mathrm{f},n}, \\ p^{n+1}=\bar{p} & \text{on} \quad \Gamma^{\mathrm{in-out}}, \\ \boldsymbol{u}^{n+1}\cdot\boldsymbol{n}^{\mathrm{f}}=D_{\tau}\boldsymbol{d}^{n+1}\cdot\boldsymbol{n}^{\mathrm{f}} & \text{on} \quad \Sigma^{n}. \end{cases} \tag{5}$$

– Solid:

$$\begin{cases} \rho^{\mathrm{s}}D_{\tau}\dot{\boldsymbol{d}}^{n+1}-\boldsymbol{\nabla}\cdot\boldsymbol{\Pi}(\boldsymbol{d}^{n+\frac{1}{2}})=\boldsymbol{0} & \text{in} \quad \Omega^{\mathrm{s}}, \\ D_{\tau}\boldsymbol{d}^{n+1}=\dot{\boldsymbol{d}}^{n+\frac{1}{2}} & \text{in} \quad \Omega^{\mathrm{s}}, \\ \boldsymbol{d}^{n+1}=\boldsymbol{0} & \text{on} \quad \Gamma^{\mathrm{d}}, \\ \boldsymbol{\Pi}(\boldsymbol{d}^{n+\frac{1}{2}})\boldsymbol{n}^{\mathrm{s}}=\boldsymbol{0} & \text{on} \quad \Gamma^{\mathrm{n}}, \\ \boldsymbol{\Pi}(\boldsymbol{d}^{n+\frac{1}{2}})\boldsymbol{n}^{\mathrm{s}}=-J^{\mathrm{f},n+1}\boldsymbol{\sigma}^{\mathrm{f}}(\tilde{\boldsymbol{u}}^{n},p^{n+1})(\boldsymbol{F}^{\mathrm{f},n+1})^{-\mathrm{T}}\boldsymbol{n}^{\mathrm{f}} & \text{on} \quad \Sigma. \end{cases} \tag{6}$$

- Explicit step (viscous-structure coupling):

$$\begin{cases} \rho^{\mathrm{f}}\dfrac{\tilde{\boldsymbol{u}}^{n+1}-\boldsymbol{u}^{n}}{\tau}\Big|_{\mathcal{A}}+\rho^{\mathrm{f}}(\tilde{\boldsymbol{u}}^{n}-\boldsymbol{w}^{n+1})\cdot\boldsymbol{\nabla}\tilde{\boldsymbol{u}}^{n+1}-2\mu\boldsymbol{\nabla}\cdot\boldsymbol{\epsilon}(\tilde{\boldsymbol{u}}^{n+1})=\boldsymbol{0} & \text{in} \quad \Omega^{\mathrm{f},n+1}, \\ 2\mu\boldsymbol{\epsilon}(\tilde{\boldsymbol{u}}^{n+1})\boldsymbol{n}^{\mathrm{f}}=\boldsymbol{0} & \text{on} \quad \Gamma^{\mathrm{in-out}}, \\ \tilde{\boldsymbol{u}}^{n+1}=D_{\tau}\boldsymbol{d}^{n} & \text{on} \quad \Sigma^{n+1}. \end{cases} \tag{7}$$

Here the scheme is presented in its velocity-correction version and with a pressure-Darcy formulation of the projection step. Other variants will also be discussed in subsection §3.4.

3 Robin Based Semi-Implicit Coupling

The main contribution of this paper concerns the discretization in space of (5)-(7), particularly, how condition $(7)_3$ is enforced at the discrete level. In [14] this condition is treated in a strong fashion. In order to enhance stability, in this work we consider a different point of view. We propose to treat weakly the explicit *viscous coupling* (6)-(7), using a Robin-Robin coupling derived from Nitsche's penalty method (see e.g. [25, 6, 7]).

3.1 Notation

In what follows, we will consider the usual Sobolev spaces $H^m(\Omega)$, $m \geq 0$, for a domain $\Omega \subset \mathbb{R}^d$. Then, for a given $X \subset \partial\Omega$ (with $\mathrm{meas}(X) > 0$), we define $H^1_X(\Omega)$ the subspace of $H^1(\Omega)$ with vanishing trace on X. In particular, we will note $V^{\mathrm{s}} \overset{\mathrm{def}}{=} [H^1_{\Gamma^{\mathrm{d}}}(\Omega^{\mathrm{s}})]^d$ and $V^{\mathrm{f}} \overset{\mathrm{def}}{=} [H^1(\Omega^{\mathrm{f}})]^d$. Finally, the scalar product in $L^2(\Omega)$ is denoted by $(\cdot,\cdot)_\Omega$ and its associated norm by $\|\cdot\|_{0,\Omega}$.

Let $\{\mathcal{T}_h^{\mathrm{f}}\}_{0<h\leq 1}$ ($\{\mathcal{T}_H^{\mathrm{s}}\}_{0<H\leq 1}$) a family of triangulations of the domain Ω^{f} (resp. Ω^{s}) satisfying the usual requirements of finite element approximations (see e.g. [11]). The subscripts $h, H \in (0,1]$ refer to the level of refinement of the triangulations. For the sake of simplicity, we assume that both families of triangulations are quasi-uniform. We define Q_h^{f} (resp. $Q_{\Gamma,h}^{\mathrm{f}}$) as an internal continuous Lagrange finite element approximation of $H^1(\Omega^{\mathrm{f}})$ (resp. $H^1_{\Gamma^{\mathrm{in-out}}}(\Omega^{\mathrm{f}})$). Similarly, V_h^{f} (resp. $V_{\Sigma,h}^{\mathrm{f}}$ and V_H^{s}) is an internal continuous Lagrange finite element approximation of V^{f} (resp. V_Σ^{f} and V^{s}). Other choices of approximation spaces are possible for the projection method, see [20] for a discussion.

In the stability analysis below, we shall make use of the following standard discrete trace-inverse inequality (see e.g. [32]):

$$||\boldsymbol{v}_h^{\mathrm{f}}||^2_{0,\partial K} \leq C_{\mathrm{ti}} h^{-1} ||\boldsymbol{v}_h^{\mathrm{f}}||^2_{0,K} \quad \forall \boldsymbol{v}_h^{\mathrm{f}} \in V_h^{\mathrm{f}} \tag{8}$$

for all $K \in \mathcal{T}_h^{\mathrm{f}}$, and with $C_{\mathrm{ti}} > 0$ a constant independent of the discretization parameter h (but that might depend on the polynomial order). Since the fluid and solid space discretizations do not necessarily match at the interface Σ, we introduce an interface matching operator $\pi_h : V_H^{\mathrm{s}}(\Sigma) \to V_h^{\mathrm{f}}(\Sigma)$, where $V_H^{\mathrm{s}}(\Sigma)$ (resp. $V_h^{\mathrm{f}}(\Sigma)$) stands for the trace finite element space associated to V_H^{s} (resp. V_h^{f}). The operator π_h can be, for instance, the standard Lagrange interpolation operator (nodal-wise matching) or a projection based operator (see e.g. [12, 18, 2]).

3.2 The Coupling Scheme

Starting from (4)-(7), our Robin based fully-discrete semi-implicit coupling scheme, applied to the non-linear coupled problem (2)-(3), reads as follows:

Algorithm 1. *Robin based semi-implicit coupling scheme (pressure-Darcy formulation)*

- Update fluid domain (mesh):

$$\begin{aligned} &\boldsymbol{d}_h^{\mathrm{f},n+1} = \mathrm{Ext}_h(\boldsymbol{d}_H^n|_\Sigma), \quad \boldsymbol{w}_h^{n+1} = D_\tau \boldsymbol{d}_h^{\mathrm{f},n+1} \quad \text{in} \quad \Omega^{\mathrm{f}}, \\ &\Omega^{\mathrm{f},n+1} = (\boldsymbol{I}_{\Omega^{\mathrm{f}}} + \boldsymbol{d}_h^{\mathrm{f},n+1})(\Omega^{\mathrm{f}}). \end{aligned} \tag{9}$$

- Implicit step (pressure-structure coupling):
  - Fluid projection sub-step:

    Find $(\boldsymbol{u}_h^{n+1}, p_h^{n+1}) \in V_h^{\mathrm{f}} \times Q_h^{\mathrm{f}}$ such that

$$\begin{cases} \dfrac{\rho^{\mathrm{f}}}{\tau}\left(\boldsymbol{u}_h^{n+1} - \widetilde{\boldsymbol{u}}_h^n, \boldsymbol{v}_h^{\mathrm{f}}\right)_{\Omega^{\mathrm{f},n}} - \left(p_h^{n+1}, \boldsymbol{\nabla}\cdot\boldsymbol{v}_h^{\mathrm{f}}\right)_{\Omega^{\mathrm{f},n}} + \left(\boldsymbol{\nabla}\cdot\boldsymbol{u}_h^{n+1}, q_h\right)_{\Omega^{\mathrm{f},n}} \\ \qquad\qquad = -\left(\bar{p}\boldsymbol{n}^{\mathrm{f}}, \boldsymbol{v}_h^{\mathrm{f}}\right)_{\Gamma^{\mathrm{in-out}}}, \\ \boldsymbol{u}_h^{n+1} = \pi_h(D_\tau \boldsymbol{d}_H^{n+1}) \quad \text{on} \quad \Sigma^n \end{cases} \tag{10}$$

    for all $(\boldsymbol{v}_h^{\mathrm{f}}, q_h) \in V_{\Sigma,h}^{\mathrm{f}} \times Q_h^{\mathrm{f}}$.

– Solid:

Find $(\boldsymbol{d}_H^{n+1}, \dot{\boldsymbol{d}}_H^{n+1}) \in [V_H^{\mathrm{s}}]^2$ such that

$$A_\tau^{\mathrm{s}}\big(\boldsymbol{d}_H^{n+1}, \dot{\boldsymbol{d}}_H^{n+1}; \boldsymbol{v}_H^{\mathrm{s}}, \dot{\boldsymbol{v}}_H^{\mathrm{s}}\big) + \frac{\gamma\mu}{h}(D_\tau \boldsymbol{d}_H^{n+1}, \boldsymbol{v}_H^{\mathrm{s}})_{\Sigma^{n+1}} = \frac{\gamma\mu}{h}(\widetilde{\boldsymbol{u}}_h^n, \boldsymbol{v}_H^{\mathrm{s}})_{\Sigma^{n+1}} - (2\mu\boldsymbol{\epsilon}(\widetilde{\boldsymbol{u}}_h^n)\boldsymbol{n}^{\mathrm{f}}, \boldsymbol{v}_H^{\mathrm{s}})_{\Sigma^{n+1}} + \big(p_h^{n+1}\boldsymbol{n}^{\mathrm{f}}, \boldsymbol{v}_H^{\mathrm{s}}\big)_{\Sigma^{n+1}} \quad (11)$$

for all $\boldsymbol{v}_H^{\mathrm{s}}, \dot{\boldsymbol{v}}_H^{\mathrm{s}} \in V_H^{\mathrm{s}}$.

- Explicit step (viscous-structure coupling):

Find $\widetilde{\boldsymbol{u}}_h^{n+1} \in V_h^{\mathrm{f}}$ such that

$$\widetilde{A}_\tau^{\mathrm{f}}\big(\widetilde{\boldsymbol{u}}_h^{n+1}, \widetilde{\boldsymbol{v}}_h^{\mathrm{f}}\big) + \frac{\gamma\mu}{h}\big(\widetilde{\boldsymbol{u}}_h^{n+1}, \widetilde{\boldsymbol{v}}_h^{\mathrm{f}}\big)_{\Sigma^{n+1}} = \frac{\gamma\mu}{h}\big(D_\tau \boldsymbol{d}_H^{n+1}, \widetilde{\boldsymbol{v}}_h^{\mathrm{f}}\big)_{\Sigma^{n+1}} + \big(2\mu\boldsymbol{\epsilon}(\widetilde{\boldsymbol{u}}_h^n)\boldsymbol{n}^{\mathrm{f}}, \widetilde{\boldsymbol{v}}_h^{\mathrm{f}}\big)_{\Sigma^{n+1}} \quad (12)$$

for all $\widetilde{\boldsymbol{v}}_h^{\mathrm{f}} \in V_h^{\mathrm{f}}$.

In the previous algorithm, Ext_h stands for a discrete counterpart of Ext, the solid mass and stiffness contribution, $A_\tau^{\mathrm{s}}\big(\boldsymbol{d}_H^{n+1}, \dot{\boldsymbol{d}}_H^{n+1}; \boldsymbol{v}_H^{\mathrm{s}}, \dot{\boldsymbol{v}}_H^{\mathrm{s}}\big)$, is given by

$$A_\tau^{\mathrm{s}}\big(\boldsymbol{d}_H^{n+1}, \dot{\boldsymbol{d}}_H^{n+1}; \boldsymbol{v}_H^{\mathrm{s}}, \dot{\boldsymbol{v}}_H^{\mathrm{s}}\big) \stackrel{\mathrm{def}}{=} \rho^s\big(D_\tau \dot{\boldsymbol{d}}_H^{n+1}, \boldsymbol{v}_H^{\mathrm{s}}\big)_{\Omega^{\mathrm{s}}} + \big(\boldsymbol{\Pi}(\boldsymbol{d}_H^{n+\frac{1}{2}}), \nabla \boldsymbol{v}_H^{\mathrm{s}}\big)_{\Omega^{\mathrm{s}}} + \rho^{\mathrm{s}}\big(\dot{\boldsymbol{d}}_H^{n+\frac{1}{2}} - D_\tau \boldsymbol{d}_H^{n+1}, \dot{\boldsymbol{v}}_H^{\mathrm{s}}\big)_{\Omega^{\mathrm{s}}},$$

while, for the fluid, $\widetilde{A}_\tau^{\mathrm{f}}\big(\widetilde{\boldsymbol{u}}_h^{n+1}, \widetilde{\boldsymbol{v}}_h^{\mathrm{f}}\big)$ is defined as

$$\begin{aligned}\widetilde{A}_\tau^{\mathrm{f}}\big(\widetilde{\boldsymbol{u}}_h^{n+1}, \widetilde{\boldsymbol{v}}_h^{\mathrm{f}}\big) \stackrel{\mathrm{def}}{=} &\frac{\rho^{\mathrm{f}}}{\tau}\left(\widetilde{\boldsymbol{u}}_h^{n+1}, \widetilde{\boldsymbol{v}}_h^{\mathrm{f}}\right)_{\Omega^{\mathrm{f},n+1}} - \frac{\rho^{\mathrm{f}}}{\tau}\left(\boldsymbol{u}_h^{n+1}, \widetilde{\boldsymbol{v}}_h^{\mathrm{f}}\right)_{\Omega^{\mathrm{f},n}} + \frac{\rho^{\mathrm{f}}}{2}\left((\boldsymbol{\nabla}\cdot\widetilde{\boldsymbol{u}}_h^n)\widetilde{\boldsymbol{u}}_h^{n+1}, \widetilde{\boldsymbol{v}}_h^{\mathrm{f}}\right)_{\Omega^{\mathrm{f},n+1}} \\ &- \rho^{\mathrm{f}}\left((\boldsymbol{\nabla}\cdot\boldsymbol{w}_h^{n+1})\widetilde{\boldsymbol{u}}_h^{n+1}, \widetilde{\boldsymbol{v}}_h^{\mathrm{f}}\right)_{\Omega^{\mathrm{f},n+1}} + \rho^{\mathrm{f}}\left((\widetilde{\boldsymbol{u}}_h^n - \boldsymbol{w}_h^{n+1})\cdot\boldsymbol{\nabla}\widetilde{\boldsymbol{u}}_h^{n+1}, \widetilde{\boldsymbol{v}}_h^{\mathrm{f}}\right)_{\Omega^{\mathrm{f},n+1}} \\ &+ \left(2\mu\boldsymbol{\epsilon}(\widetilde{\boldsymbol{u}}_h^{n+1}), \boldsymbol{\epsilon}(\widetilde{\boldsymbol{v}}_h^{\mathrm{f}})\right)_{\Omega^{\mathrm{f},n+1}}.\end{aligned} \quad (13)$$

Finally, $\gamma > 0$ is a dimensionless parameter. Some remarks are now in order.

Remark 3.1 *In Algorithm 1, the kinematic condition* $(5)_4$ *is strongly imposed (as in [14]). However, now the coupling between the solid* (6) *and viscous* (7) *sub-steps is weakly enforced.*

Remark 3.2 *Note that, in* (10)*, we impose* $\boldsymbol{u}_h^{n+1} = \pi_h(D_\tau \boldsymbol{d}_H^{n+1})$ *on* Σ^n *(instead of* $(5)_4$*) which is also optimal in the framework of finite element approximations (see [19]).*

The interface weak coupling between steps (11) and (12) differs from the commonly used Nitsche's interface formulations (see e.g. [6, 22, 8, 1]). In particular, the interface mortaring in (12) does not contain the classical Nitsche's symmetrizing term

$$-\big(\widetilde{\boldsymbol{u}}_h^{n+1} - D_\tau \boldsymbol{d}_H^{n+1}, 2\mu\boldsymbol{\epsilon}(\widetilde{\boldsymbol{v}}_h^{\mathrm{f}})\boldsymbol{n}^{\mathrm{f}}\big)_{\Sigma^{n+1}}.$$

Note that this simplification does not compromise symmetry, since (as in [8, 1]) the Nitsche's consistency term

$$-\big(2\mu\boldsymbol{\epsilon}(\widetilde{\boldsymbol{u}}_h^n)\boldsymbol{n}^{\mathrm{f}}, \widetilde{\boldsymbol{v}}_h^{\mathrm{f}} - \boldsymbol{v}_H^{\mathrm{s}}\big)_{\Sigma^{n+1}},$$

is evaluated at the previous time step.

A major consequence of the previous observation is that the space continuous counterpart of the coupling between sub-steps (11) and (12) can be formally written as

$$\left.\begin{aligned} \frac{\gamma\mu}{h} D_\tau \boldsymbol{d}^{n+1} + \boldsymbol{\sigma}^{\mathrm{s}}(\boldsymbol{d}^{n+\frac{1}{2}})\boldsymbol{n}^{\mathrm{s}} &= \frac{\gamma\mu}{h}\tilde{\boldsymbol{u}}^n - 2\mu\boldsymbol{\epsilon}(\tilde{\boldsymbol{u}}^n)\boldsymbol{n}^{\mathrm{f}} + p^{n+1}\boldsymbol{n}^{\mathrm{f}} \\ \frac{\gamma\mu}{h}\tilde{\boldsymbol{u}}^{n+1} + 2\mu\boldsymbol{\epsilon}(\tilde{\boldsymbol{u}}^{n+1})\boldsymbol{n}^{\mathrm{f}} &= \frac{\gamma\mu}{h} D_\tau \boldsymbol{d}^{n+1} + 2\mu\boldsymbol{\epsilon}(\tilde{\boldsymbol{u}}^n)\boldsymbol{n}^{\mathrm{f}} \end{aligned}\right\} \quad \text{on} \quad \Sigma^{n+1}, \tag{14}$$

which corresponds to an explicit Robin-Robin coupling between sub-steps (11) and (12). Note that the scaling $\gamma\mu/h$ of the Robin parameter, appearing in (14), coincides with the scaling of the original Nitsche's penalty method (see e.g. [25, 6, 7, 8]), which is based on optimal convergence and energy arguments. However, it drastically differs from the heuristic Robin-Robin scaling proposed in [4], based on simplified models and which aims at accelerating partitioned iterative solution methods within a fully implicit coupling framework.

3.3 Pressure Load Computation

In (11), the pressure contribution of the fluid load at the interface $\big(p_h^{n+1}\boldsymbol{n}^{\mathrm{f}}, \boldsymbol{v}_H^{\mathrm{s}}\big)_{\Sigma^{n+1}}$ is computed as a face-wise integral. This approach is referred in the numerical experiments as FWI (Face-Wise Integral). Nevertheless, the theoretical stability analysis (carried out in section §4) calls for the following residual based approximation of the pressure interface integral:

$$\begin{aligned} \big\langle \mathcal{R}(\boldsymbol{u}_h^{n+1}, \tilde{\boldsymbol{u}}_h^n, p_h^{n+1}), \mathcal{L}_h(\boldsymbol{v}_H^{\mathrm{s}})\big\rangle \overset{\mathrm{def}}{=} \frac{\rho^{\mathrm{f}}}{\tau}\big(\boldsymbol{u}_h^{n+1} - \tilde{\boldsymbol{u}}_h^n, \mathcal{L}_h(\boldsymbol{v}_H^{\mathrm{s}})\big)_{\Omega^{\mathrm{f},n+1}} \\ - \big(p_h^{n+1}, \nabla\cdot(\mathcal{L}_h(\boldsymbol{v}_H^{\mathrm{s}}))\big)_{\Omega^{\mathrm{f},n+1}}, \end{aligned} \tag{15}$$

with $\mathcal{L}_h \overset{\mathrm{def}}{=} \mathcal{L}_h^{\mathrm{f}} \circ \pi_h$ and $\mathcal{L}_h^{\mathrm{f}} : V_h^{\mathrm{f}}(\Sigma) \to V_h^{\mathrm{f}}$ is a given discrete fluid lifting operator such that

$$\mathcal{L}_h^{\mathrm{f}}(\boldsymbol{v}_h^{\mathrm{f}}) = \begin{cases} \boldsymbol{v}_h^{\mathrm{f}} & \text{on} \quad \Sigma, \\ \boldsymbol{0} & \text{on} \quad \Gamma^{\mathrm{in-out}}. \end{cases}$$

Moreover, for the stability analysis reported in subsection §4.3.1, we shall assume that the following continuity estimate holds

$$\|\mathcal{L}_h^{\mathrm{f}}(\boldsymbol{v}_h^{\mathrm{f}})\|_{0,\Omega^{\mathrm{f}}}^2 \le C_{\mathcal{L}} h \|\boldsymbol{v}_h^{\mathrm{f}}\|_{0,\Sigma}^2, \tag{16}$$

with $C_{\mathcal{L}} > 0$ a constant depending only on the fluid polynomial order and the mesh regularity. Let us emphasize that (16) holds for the discrete lifting operator commonly used in practice (see e.g. [12, 14]).

In the numerical experiments, the method resulting from replacing in (11) the interface integral $\big(p_h^{n+1}\boldsymbol{n}^{\mathrm{f}}, \boldsymbol{v}_H^{\mathrm{s}}\big)_{\Sigma^{n+1}}$ by $\big\langle \mathcal{R}(\boldsymbol{u}_h^{n+1}, \tilde{\boldsymbol{u}}_h^n, p_h^{n+1}), \mathcal{L}_h(\boldsymbol{v}_H^{\mathrm{s}})\big\rangle$ will be indicated as VR (Variational-Residual).

3.4 Variants

In this subsection we discuss a couple of variants of the semi-implicit coupling scheme (9)-(12).

3.4.1 Pressure-Poisson Formulation

As usual, instead of the pressure-Darcy formulation (10), the intermediate velocity $\boldsymbol{u}_h^{n+1}$ can be eliminated by rewriting the projection step as a pressure-Poisson equation (with a Neumann condition on the interface). Thus, (10) becomes

$$\left\{\begin{array}{l} \dfrac{\tau}{\rho^{\mathrm{f}}}\left(\boldsymbol{\nabla} p_h^{n+1}, \boldsymbol{\nabla} q_h\right)_{\Omega^{\mathrm{f},n}} = -\left(\boldsymbol{\nabla}\cdot\widetilde{\boldsymbol{u}}_h^n, q_h\right)_{\Omega^{\mathrm{f},n}} - \left(\left(\pi_h(D_\tau \boldsymbol{d}_H^{n+1}) - \widetilde{\boldsymbol{u}}_h^n\right)\cdot\boldsymbol{n}^{\mathrm{f}}, q_h\right)_{\Sigma^n}, \\ \qquad\qquad p_h^{n+1} = \bar{p} \quad \text{on} \quad \Gamma^{\mathrm{in-out}} \end{array}\right. \tag{17}$$

for all $q_h \in Q^{\mathrm{f}}_{\Gamma,h}$, and the intermediate velocity $\widetilde{\boldsymbol{u}}_h^n - \dfrac{\tau}{\rho^{\mathrm{f}}}\boldsymbol{\nabla} p_h^{n+1}$ replaces $\boldsymbol{u}_h^{n+1}$ in (13).

Note that, due to the hybrid treatment of the kinematic conditions $(5)_4$ and $(7)_3$ (see Remark 3.1), the interface integral in $(17)_1$ couples two different kinds of interface mortaring: one based on the (solid-to-fluid) matching operator π_h and the other on the viscous Robin coupling. Thus, as suggested by the theoretical stability analysis carried out in subsection §4.3.1, this hybrid mortaring requires a specific integration of the interface terms in (11) and (12). More precisely, (11) has to be replaced by

$$\left\{\begin{array}{l} A_\tau^{\mathrm{s}}\left(\boldsymbol{d}_H^{n+1}, \dot{\boldsymbol{d}}_H^{n+1}; \boldsymbol{v}_H^{\mathrm{s}}, \dot{\boldsymbol{v}}_H^{\mathrm{s}}\right) + \dfrac{\gamma\mu}{h}\left(\pi_h(D_\tau \boldsymbol{d}_H^{n+1}) - \widetilde{\boldsymbol{u}}_h^n, \pi_h(\boldsymbol{v}_H^{\mathrm{s}})\right)_{\Sigma^{n+1}} \\ \qquad\qquad = -\left(2\mu\boldsymbol{\epsilon}(\widetilde{\boldsymbol{u}}_h^n)\boldsymbol{n}^{\mathrm{f}}, \pi_h(\boldsymbol{v}_H^{\mathrm{s}})\right)_{\Sigma^{n+1}} + \left(p_h^{n+1}\boldsymbol{n}^{\mathrm{f}}, \boldsymbol{v}_H^{\mathrm{s}}\right)_{\Sigma^{n+1}} \end{array}\right. \tag{18}$$

for all $\boldsymbol{v}_H^{\mathrm{s}}, \dot{\boldsymbol{v}}_H^{\mathrm{s}} \in V_H^{\mathrm{s}}$, and (12) by

$$\widetilde{A}_\tau^{\mathrm{f}}\left(\widetilde{\boldsymbol{u}}_h^{n+1}, \widetilde{\boldsymbol{v}}_h^{\mathrm{f}}\right) + \frac{\gamma\mu}{h}\left(\widetilde{\boldsymbol{u}}_h^{n+1} - \pi_h(D_\tau \boldsymbol{d}_H^{n+1}), \widetilde{\boldsymbol{v}}_h^{\mathrm{f}}\right)_{\Sigma^{n+1}} = \left(2\mu\boldsymbol{\epsilon}(\widetilde{\boldsymbol{u}}_h^n)\boldsymbol{n}^{\mathrm{f}}, \widetilde{\boldsymbol{v}}_h^{\mathrm{f}}\right)_{\Sigma^{n+1}} \tag{19}$$

for all $\widetilde{\boldsymbol{v}}_h^{\mathrm{f}} \in V_h^{\mathrm{f}}$.

Note that the modifications (18) and (19) are only suggested when dealing with non-matching fluid-solid discretizations and when using the pressure-Poisson version of the Chorin-Temam scheme.

Remark 3.3 *In the pressure-Poisson version of Algorithm 1 combined with a VR based pressure load computation, the intermediate velocity* $\boldsymbol{u}_h^{n+1} \in V_h^{\mathrm{f}}$*, required by* (15)*, is the solution of*

$$\begin{aligned} \frac{\rho^f}{\tau}\left(\boldsymbol{u}_h^{n+1} - \tilde{\boldsymbol{u}}_h^n, \boldsymbol{v}_h^{\mathrm{f}}\right)_{\Omega^{\mathrm{f},n}} &= -\left(\boldsymbol{\nabla} p_h^{n+1}, \boldsymbol{v}_h^{\mathrm{f}}\right)_{\Omega^{\mathrm{f},n}}, \\ \boldsymbol{u}_h^{n+1} &= \pi_h(D_\tau \boldsymbol{d}_H^{n+1}) \quad \textit{on} \quad \Sigma^n \end{aligned}$$

for all $\boldsymbol{v}_h^{\mathrm{f}} \in V^{\mathrm{f}}_{\Sigma,h}$.

3.4.2 Pressure-Correction Formulation

In Algorithm 1 we have used the velocity-correction version of the Chorin-Temam projection scheme. However, as in [14], we could also have considered the pressure-correction version by switching the explicit and implicit steps (see Remark 4.4): $\boldsymbol{u}_h^{n+1}$ has to be replaced by $\boldsymbol{u}_h^n$ in $\widetilde{A}_\tau^{\mathrm{f}}\big(\widetilde{\boldsymbol{u}}_h^{n+1}, \widetilde{\boldsymbol{v}}_h^{\mathrm{f}}\big)$, step (12) by

$$\widetilde{A}_\tau^{\mathrm{f}}\big(\widetilde{\boldsymbol{u}}_h^{n+1}, \widetilde{\boldsymbol{v}}_h^{\mathrm{f}}\big) + \frac{\gamma\mu}{h}\big(\widetilde{\boldsymbol{u}}_h^{n+1}, \widetilde{\boldsymbol{v}}_h^{\mathrm{f}}\big)_{\Sigma^{n+1}} = \frac{\gamma\mu}{h}\big(D_\tau \boldsymbol{d}_H^n, \widetilde{\boldsymbol{v}}_h^{\mathrm{f}}\big)_{\Sigma^{n+1}} + \big(2\mu\boldsymbol{\epsilon}(\widetilde{\boldsymbol{u}}_h^n)\boldsymbol{n}^{\mathrm{f}}, \widetilde{\boldsymbol{v}}_h^{\mathrm{f}}\big)_{\Sigma^{n+1}} \tag{20}$$

for all $\widetilde{\boldsymbol{v}}_h^{\mathrm{f}} \in V_h^{\mathrm{f}}$, step (10) by

$$\begin{cases} \dfrac{\rho^{\mathrm{f}}}{\tau}\Big(\boldsymbol{u}_h^{n+1} - \widetilde{\boldsymbol{u}}_h^{n+1}, \boldsymbol{v}_h^{\mathrm{f}}\Big)_{\Omega^{\mathrm{f},n+1}} - \big(p_h^{n+1}, \boldsymbol{\nabla}\cdot\boldsymbol{v}_h^{\mathrm{f}}\big)_{\Omega^{\mathrm{f},n+1}} + \big(\boldsymbol{\nabla}\cdot\boldsymbol{u}_h^{n+1}, q_h\big)_{\Omega^{\mathrm{f},n+1}} \\ \qquad\qquad = -\big(\bar{p}\boldsymbol{n}^{\mathrm{f}}, \boldsymbol{v}_h^{\mathrm{f}}\big)_{\Gamma^{\mathrm{in-out}}}, \\ \boldsymbol{u}_h^{n+1} = \pi_h(D_\tau \boldsymbol{d}_H^{n+1}) \quad \text{on} \quad \Sigma^{n+1} \end{cases} \tag{21}$$

for all $(\boldsymbol{v}_h^{\mathrm{f}}, q_h) \in V_{\Sigma,h}^{\mathrm{f}} \times Q_h^{\mathrm{f}}$, and finally step (11) becomes

$$\begin{aligned} A_\tau^{\mathrm{s}}\big(\boldsymbol{d}_H^{n+1}, \dot{\boldsymbol{d}}_H^{n+1}; \boldsymbol{v}_H^{\mathrm{s}}, \dot{\boldsymbol{v}}_H^{\mathrm{s}}\big) + \frac{\gamma\mu}{h}(D_\tau \boldsymbol{d}_H^{n+1}, \boldsymbol{v}_H^{\mathrm{s}})_{\Sigma^{n+1}} &= \frac{\gamma\mu}{h}(\widetilde{\boldsymbol{u}}_h^{n+1}, \boldsymbol{v}_H^{\mathrm{s}})_{\Sigma^{n+1}} \\ &\quad - (2\mu\boldsymbol{\epsilon}(\widetilde{\boldsymbol{u}}_h^n)\boldsymbol{n}^{\mathrm{f}}, \boldsymbol{v}_H^{\mathrm{s}})_{\Sigma^{n+1}} + \big(p_h^{n+1}\boldsymbol{n}^{\mathrm{f}}, \boldsymbol{v}_H^{\mathrm{s}}\big)_{\Sigma^{n+1}} \end{aligned} \tag{22}$$

for all $\boldsymbol{v}_H^{\mathrm{s}}, \dot{\boldsymbol{v}}_H^{\mathrm{s}} \in V_H^{\mathrm{s}}$.

Remark 3.4 *The extension of our approach to the semi-implicit coupling framework reported in [27, 5] is not straightforward. Note that our Robin based semi-implicit coupling fully exploits the splitting* (5)-(7) *induced by the Chorin-Temam scheme, which allows a hybrid treatment of the kinematic coupling conditions* $(5)_4$ *and* $(7)_3$*. However, in [27, 5] the splitting is performed directly on the fully discrete linearized system, by using appropriate inexact LU factorizations, with a predefined treatment of the kinematic coupling.*

4 Stability Analysis

In this section, the stability analysis of our Robin based semi-implicit coupling is carried out on a linearized version of problem (2)-(3). Both the pressure-Darcy and pressure-Poisson formulations are considered and analyzed.

4.1 A Simplified Model Problem

The fluid is described by the Stokes equations in a fixed domain $\Omega^{\mathrm{f}} \subset \mathbb{R}^d$, $d = 2, 3$. For the structure, we consider the classical linear elastodynamics equations, in the solid domain $\Omega^{\mathrm{s}} \subset \mathbb{R}^d$. We still denote by $\Sigma \stackrel{\text{def}}{=} \partial\Omega^{\mathrm{s}} \cap \partial\Omega^{\mathrm{f}}$ the fluid-structure interface. Then, our linearized fluid-structure problem reads as follows:

Find the fluid velocity $\boldsymbol{u} : \Omega^{\mathrm{f}} \times \mathbb{R}^+ \to \mathbb{R}^d$, the fluid pressure $p : \Omega^{\mathrm{f}} \times \mathbb{R}^+ \to \mathbb{R}$ and the structure displacement $\boldsymbol{d} : \Omega^{\mathrm{s}} \times \mathbb{R}^+ \to \mathbb{R}^d$ such that:

$$\begin{cases} \rho^{\mathrm{f}} \partial_t \boldsymbol{u} - \boldsymbol{\nabla} \cdot \boldsymbol{\sigma}^{\mathrm{f}}(\boldsymbol{u}, p) = \boldsymbol{0} & \text{in} \quad \Omega^{\mathrm{f}}, \\ \boldsymbol{\nabla} \cdot \boldsymbol{u} = 0 & \text{in} \quad \Omega^{\mathrm{f}}, \\ \boldsymbol{\sigma}^{\mathrm{f}}(\boldsymbol{u}, p)\boldsymbol{n}^{\mathrm{f}} = -\bar{p}\boldsymbol{n}^{\mathrm{f}} & \text{on} \quad \Gamma^{\mathrm{in-out}}, \\ \rho^{\mathrm{s}} \partial_{tt} \boldsymbol{d} - \boldsymbol{\nabla} \cdot \boldsymbol{\sigma}^{\mathrm{s}}(\boldsymbol{d}) = \boldsymbol{0} & \text{in} \quad \Omega^{\mathrm{s}}, \\ \boldsymbol{d} = \boldsymbol{0} & \text{on} \quad \Gamma^{\mathrm{d}}, \\ \boldsymbol{\sigma}^{\mathrm{s}}(\boldsymbol{d})\boldsymbol{n}^{\mathrm{s}} = \boldsymbol{0} & \text{on} \quad \Gamma^{\mathrm{n}}, \\ \boldsymbol{u} = \partial_t \boldsymbol{d} & \text{on} \quad \Sigma, \\ \boldsymbol{\sigma}^{\mathrm{s}}(\boldsymbol{d})\boldsymbol{n}^{\mathrm{s}} = -\boldsymbol{\sigma}^{\mathrm{f}}(\boldsymbol{u}, p)\boldsymbol{n}^{\mathrm{f}} & \text{on} \quad \Sigma. \end{cases} \tag{23}$$

System (23), though simplified, contains the key features of more complex fluid-structure problems involving an incompressible fluid, with respect to the stability of the coupling schemes (see e.g. [9, 14, 8]).

4.2 Semi-Implicit Coupling With Pressure-Darcy Formulation

Algorithm 1 applied to the linearized problem (23) yields:

- Implicit step (pressure-solid coupling):
  Find $(\boldsymbol{u}_h^{n+1}, p_h^{n+1}, \boldsymbol{d}_H^{n+1}, \dot{\boldsymbol{d}}_H^{n+1}) \in V_h^{\mathrm{f}} \times Q_h^{\mathrm{f}} \times [V_H^{\mathrm{s}}]^2$ such that

$$\begin{cases} \dfrac{\rho^{\mathrm{f}}}{\tau}\big(\boldsymbol{u}_h^{n+1} - \tilde{\boldsymbol{u}}_h^n, \boldsymbol{v}_h^{\mathrm{f}}\big)_{\Omega^{\mathrm{f}}} - \big(p_h^{n+1}, \boldsymbol{\nabla} \cdot \boldsymbol{v}_h^{\mathrm{f}}\big)_{\Omega^{\mathrm{f}}} + \big(q_h, \boldsymbol{\nabla} \cdot \boldsymbol{u}_h^{n+1}\big)_{\Omega^{\mathrm{f}}} \\ \qquad = -\big(\bar{p}\boldsymbol{v}_h^{\mathrm{f}}, \boldsymbol{n}^{\mathrm{f}}\big)_{\Gamma^{\mathrm{in-out}}} \quad \forall (\boldsymbol{v}_h^{\mathrm{f}}, q_h) \in V_{\Sigma,h}^{\mathrm{f}} \times Q_h^{\mathrm{f}}, \\ \qquad\qquad \boldsymbol{u}_h^{n+1} = \pi_h(D_\tau \boldsymbol{d}_H^{n+1}) \quad \text{on} \quad \Sigma. \end{cases} \tag{24}$$

$$\begin{cases} \dfrac{\rho^{\mathrm{s}}}{\tau}\big(\dot{\boldsymbol{d}}_H^{n+1} - \dot{\boldsymbol{d}}_H^n, \boldsymbol{v}_H^{\mathrm{s}}\big)_{\Omega^{\mathrm{s}}} + a^{\mathrm{s}}\big(\boldsymbol{d}_H^{n+\frac{1}{2}}, \boldsymbol{v}_H^{\mathrm{s}}\big) + \dfrac{\gamma\mu}{h}\big(D_\tau \boldsymbol{d}_H^{n+1} - \tilde{\boldsymbol{u}}_h^n, \boldsymbol{v}_H^{\mathrm{s}}\big)_\Sigma \\ = -2\mu\big(\boldsymbol{\epsilon}(\tilde{\boldsymbol{u}}_h^n)\boldsymbol{n}^{\mathrm{f}}, \boldsymbol{v}_H^{\mathrm{s}}\big)_\Sigma - \big\langle \mathcal{R}(\boldsymbol{u}_h^{n+1}, \tilde{\boldsymbol{u}}_h^n, p_h^{n+1}), \mathcal{L}_h(\boldsymbol{v}_H^{\mathrm{s}}) \big\rangle, \quad \forall \boldsymbol{v}_H^{\mathrm{s}} \in V_H^{\mathrm{s}}, \\ \qquad\qquad D_\tau \boldsymbol{d}_H^{n+1} = \dot{\boldsymbol{d}}_H^{n+\frac{1}{2}}, \quad \text{in} \quad \Omega^{\mathrm{s}}. \end{cases} \tag{25}$$

- Explicit step (viscous-solid coupling):
  Find $\tilde{\boldsymbol{u}}_h^{n+1} \in V_h^{\mathrm{f}}$ such that

$$\begin{cases} \dfrac{\rho^{\mathrm{f}}}{\tau}\big(\tilde{\boldsymbol{u}}_h^{n+1} - \boldsymbol{u}_h^{n+1}, \tilde{\boldsymbol{v}}_h^{\mathrm{f}}\big)_{\Omega^{\mathrm{f}}} + 2\mu\big(\boldsymbol{\epsilon}(\tilde{\boldsymbol{u}}_h^{n+1}), \boldsymbol{\epsilon}(\tilde{\boldsymbol{v}}_h^{\mathrm{f}})\big)_{\Omega^{\mathrm{f}}} + \dfrac{\gamma\mu}{h}\big(\tilde{\boldsymbol{u}}_h^{n+1} - D_\tau \boldsymbol{d}_H^{n+1}, \tilde{\boldsymbol{v}}_h^{\mathrm{f}}\big)_\Sigma \\ \qquad\qquad = 2\mu\big(\boldsymbol{\epsilon}(\tilde{\boldsymbol{u}}_h^n)\boldsymbol{n}^{\mathrm{f}}, \tilde{\boldsymbol{v}}_h^{\mathrm{f}}\big)_\Sigma \quad \forall \tilde{\boldsymbol{v}}_h^{\mathrm{f}} \in V_h^{\mathrm{f}}. \end{cases} \tag{26}$$

In (25), $a^{\mathrm{s}}(\cdot,\cdot)$ stands for the solid stiffness symmetric bilinear form. Note that we have considered a VR (Variational-Residual) based approximation of the pressure stresses at the interface, which in this case is given by:

$$\left\langle \mathcal{R}(\boldsymbol{u}_h^{n+1}, \tilde{\boldsymbol{u}}_h^n, p_h^{n+1}), \mathcal{L}_h(\boldsymbol{v}_H^{\mathrm{s}}) \right\rangle \stackrel{\mathrm{def}}{=} \frac{\rho^{\mathrm{f}}}{\tau}\left(\boldsymbol{u}_h^{n+1} - \tilde{\boldsymbol{u}}_h^n, \mathcal{L}_h(\boldsymbol{v}_H^{\mathrm{s}})\right)_{\Omega^{\mathrm{f}}} - \left(p_h^{n+1}, \nabla\cdot(\mathcal{L}_h(\boldsymbol{v}_H^{\mathrm{s}}))\right)_{\Omega^{\mathrm{f}}}$$

for all $\boldsymbol{v}_H^{\mathrm{s}} \in V_H^{\mathrm{s}}$.

4.2.1 Energy Based Stability Analysis

In this section, we show that the semi-implicit scheme (24)-(26) is conditionally stable irrespectively of the added-mass effect.

Let us define the energy of the discrete coupled system, at time $t_n \stackrel{\mathrm{def}}{=} n\tau$, as:

$$E^n = \frac{\rho^{\mathrm{f}}}{2}\|\tilde{\boldsymbol{u}}_h^n\|_{0,\Omega^{\mathrm{f}}}^2 + \frac{\rho^{\mathrm{s}}}{2}\|\dot{\boldsymbol{d}}_H^n\|_{0,\Omega^{\mathrm{s}}}^2 + \frac{1}{2}a^{\mathrm{s}}(\boldsymbol{d}_H^n, \boldsymbol{d}_H^n).$$

Theorem 4.1 *Assume that the system is isolated, i.e. $\bar{p} = 0$ on $\Gamma^{\mathrm{in-out}}$, and let $\left\{(\tilde{\boldsymbol{u}}_h^n, \boldsymbol{u}_h^n, p_h^n, \boldsymbol{d}_H^n, \dot{\boldsymbol{d}}_H^n)\right\}_{n\geq 0}$ be solution of (24)-(26). Then, the following discrete energy estimate holds:*

$$E^n + \mu\tau\sum_{m=0}^{n-1}\|\boldsymbol{\epsilon}(\tilde{\boldsymbol{u}}_h^{m+1})\|_{0,\Omega^{\mathrm{f}}}^2 + (\gamma - 2C_{\mathrm{ti}})\frac{\mu\tau}{2h}\sum_{m=0}^{n}\|\tilde{\boldsymbol{u}}_h^{m+1} - D_\tau\boldsymbol{d}_H^{m+1}\|_{0,\Sigma}^2 + \frac{\gamma\mu\tau}{2h}\|\tilde{\boldsymbol{u}}_h^n\|_{0,\Sigma}^2 \leq E^0 + \mu\tau\|\boldsymbol{\epsilon}(\tilde{\boldsymbol{u}}_h^0)\|_{0,\Omega^{\mathrm{f}}}^2 + \frac{\gamma\mu\tau}{2h}\|\tilde{\boldsymbol{u}}_h^0\|_{0,\Sigma}^2. \quad (27)$$

Therefore, the semi-implicit coupling scheme (24)-(26) *is stable, in the energy-norm, under the conditions:*

$$\gamma \geq 2C_{\mathrm{ti}}, \quad \gamma\mu\tau = \mathcal{O}(h). \quad (28)$$

Proof. We proceed by testing equations (24)-(26) with

$$\boldsymbol{v}_h^{\mathrm{f}} = \tau(\boldsymbol{u}_h^{n+1} - \mathcal{L}_h(D_\tau\boldsymbol{d}_H^{n+1})), \quad q_h = \tau p_h^{n+1}, \quad \boldsymbol{v}_H^{\mathrm{s}} = \tau D_\tau\boldsymbol{d}_H^{n+1}, \quad \tilde{\boldsymbol{v}}_h^{\mathrm{f}} = \tau\tilde{\boldsymbol{u}}_h^{n+1},$$

which are all admissible test functions. Therefore, using the identity $(a-b,a) = \frac{1}{2}\|a\|^2 - \frac{1}{2}\|b\|^2 + \frac{1}{2}\|a-b\|^2$, from (24) we get

$$\frac{\rho^{\mathrm{f}}}{2}\left[\|\boldsymbol{u}_h^{n+1}\|_{0,\Omega^{\mathrm{f}}}^2 - \|\tilde{\boldsymbol{u}}_h^n\|_{0,\Omega^{\mathrm{f}}}^2\right] - \tau\left\langle \mathcal{R}(\boldsymbol{u}_h^{n+1}, \tilde{\boldsymbol{u}}_h^n, p_h^{n+1}), \mathcal{L}_h(D_\tau\boldsymbol{d}_H^{n+1})\right\rangle \leq 0.$$

Similarly, from (25) we obtain

$$\frac{\rho^{\mathrm{s}}}{2}\left[\|\dot{\boldsymbol{d}}_H^{n+1}\|_{0,\Omega^{\mathrm{s}}}^2 - \|\dot{\boldsymbol{d}}_H^n\|_{0,\Omega^{\mathrm{s}}}^2\right] + \frac{1}{2}\left[a^{\mathrm{s}}(\boldsymbol{d}_H^{n+1}, \boldsymbol{d}_H^{n+1}) - a^{\mathrm{s}}(\boldsymbol{d}_H^n, \boldsymbol{d}_H^n)\right] + 2\mu\tau\left(\boldsymbol{\epsilon}(\tilde{\boldsymbol{u}}_h^n)\boldsymbol{n}^{\mathrm{f}}, D_\tau\boldsymbol{d}_H^{n+1}\right)_\Sigma + \frac{\gamma\mu\tau}{h}\left(D_\tau\boldsymbol{d}_H^{n+1} - \tilde{\boldsymbol{u}}_h^n, D_\tau\boldsymbol{d}_H^{n+1}\right)_\Sigma + \tau\left\langle \mathcal{R}(\boldsymbol{u}_h^{n+1}, \tilde{\boldsymbol{u}}_h^n, p_h^{n+1}), \mathcal{L}_h(D_\tau\boldsymbol{d}_H^{n+1})\right\rangle = 0, \quad (29)$$

and (26) yields

$$\frac{\rho^{\mathrm{f}}}{2}\left[\|\tilde{\boldsymbol{u}}_h^{n+1}\|_{0,\Omega^{\mathrm{f}}}^2-\|\boldsymbol{u}_h^{n+1}\|_{0,\Omega^{\mathrm{f}}}^2\right]+2\mu\tau\|\boldsymbol{\epsilon}(\tilde{\boldsymbol{u}}_h^{n+1})\|_{0,\Omega^{\mathrm{f}}}^2-2\mu\tau\big(\boldsymbol{\epsilon}(\tilde{\boldsymbol{u}}_h^{n})\boldsymbol{n}^{\mathrm{f}},\tilde{\boldsymbol{u}}_h^{n+1}\big)_\Sigma + \frac{\gamma\mu\tau}{h}\big(\tilde{\boldsymbol{u}}_h^{n+1}-D_\tau\boldsymbol{d}_H^{n+1},\tilde{\boldsymbol{u}}_h^{n+1}\big)_\Sigma\leq 0.$$

By summation of these three inequalities, we obtain

$$E^{n+1}-E^n+2\mu\tau\|\boldsymbol{\epsilon}(\tilde{\boldsymbol{u}}_h^{n+1})\|_{0,\Omega^{\mathrm{f}}}\underbrace{-2\mu\tau\big(\boldsymbol{\epsilon}(\tilde{\boldsymbol{u}}_h^{n})\boldsymbol{n}^{\mathrm{f}},\tilde{\boldsymbol{u}}_h^{n+1}-D_\tau\boldsymbol{d}_H^{n+1}\big)_\Sigma}_{\mathcal{T}_2}$$
$$+\underbrace{\frac{\gamma\mu\tau}{h}\Big[\big(D_\tau\boldsymbol{d}_H^{n+1}-\tilde{\boldsymbol{u}}_h^{n},D_\tau\boldsymbol{d}_H^{n+1}\big)_\Sigma+\big(\tilde{\boldsymbol{u}}_h^{n+1}-D_\tau\boldsymbol{d}_H^{n+1},\tilde{\boldsymbol{u}}_h^{n+1}\big)_\Sigma\Big]}_{\mathcal{T}_1}\leq 0. \quad (30)$$

We now estimate terms $\mathcal{T}_1$ and $\mathcal{T}_2$ separately.

We first consider term $\mathcal{T}_1$ by noting that

$$\mathcal{T}_1=\frac{\gamma\mu\tau}{h}\left[\|\tilde{\boldsymbol{u}}_h^{n+1}-D_\tau\boldsymbol{d}_H^{n+1}\|_{0,\Sigma}^2+\big(\tilde{\boldsymbol{u}}_h^{n+1}-\tilde{\boldsymbol{u}}_h^{n},D_\tau\boldsymbol{d}_H^{n+1}\big)_\Sigma\right]. \quad (31)$$

As in [8], the last term in (31) can be treated as follows

$$\begin{aligned}\big(\tilde{\boldsymbol{u}}_h^{n+1}-\tilde{\boldsymbol{u}}_h^{n},D_\tau\boldsymbol{d}_H^{n+1}\big)_\Sigma=&\big(\tilde{\boldsymbol{u}}_h^{n+1}-\tilde{\boldsymbol{u}}_h^{n},D_\tau\boldsymbol{d}_H^{n+1}-\tilde{\boldsymbol{u}}_h^{n+1}\big)_\Sigma+\big(\tilde{\boldsymbol{u}}_h^{n+1}-\tilde{\boldsymbol{u}}_h^{n},\tilde{\boldsymbol{u}}_h^{n+1}\big)_\Sigma\\ \geq&-\frac{1}{2}\|\tilde{\boldsymbol{u}}_h^{n+1}-\tilde{\boldsymbol{u}}_h^{n}\|_{0,\Sigma}^2-\frac{1}{2}\|D_\tau\boldsymbol{d}_H^{n+1}-\tilde{\boldsymbol{u}}_h^{n+1}\|_{0,\Sigma}^2\\ &+\frac{1}{2}\|\tilde{\boldsymbol{u}}_h^{n+1}\|_{0,\Sigma}^2-\frac{1}{2}\|\tilde{\boldsymbol{u}}_h^{n}\|_{0,\Sigma}^2+\frac{1}{2}\|\tilde{\boldsymbol{u}}_h^{n+1}-\tilde{\boldsymbol{u}}_h^{n}\|_{0,\Sigma}^2\\ \geq&\frac{1}{2}\big(\|\tilde{\boldsymbol{u}}_h^{n+1}\|_{0,\Sigma}^2-\|\tilde{\boldsymbol{u}}_h^{n}\|_{0,\Sigma}^2-\|\tilde{\boldsymbol{u}}_h^{n+1}-D_\tau\boldsymbol{d}_H^{n+1}\|_{0,\Sigma}^2\big),\end{aligned}$$

which leads to the bound

$$\mathcal{T}_1\geq\frac{\gamma\mu\tau}{2h}\left[\|\tilde{\boldsymbol{u}}_h^{n+1}-D_\tau\boldsymbol{d}_H^{n+1}\|_{0,\Sigma}^2+\|\tilde{\boldsymbol{u}}_h^{n+1}\|_{0,\Sigma}^2-\|\tilde{\boldsymbol{u}}_h^{n}\|_{0,\Sigma}^2\right]. \quad (32)$$

For term $\mathcal{T}_2$, by combining the Cauchy-Schwarz and Young inequalities with (8) we get

$$\mathcal{T}_2\geq-\mu\tau\|\boldsymbol{\epsilon}(\tilde{\boldsymbol{u}}_h^{n})\|_{0,\Omega^{\mathrm{f}}}^2-\frac{\mu\tau C_{\mathrm{ti}}}{h}\|\tilde{\boldsymbol{u}}_h^{n+1}-D_\tau\boldsymbol{d}_H^{n+1}\|_{0,\Sigma}^2. \quad (33)$$

Finally, we recover (27) by inserting (32) and (33) into (30), replacing n by m and summing over $m=0,\ldots,n-1$. This completes the proof.

Remark 4.2 *Since the stability condition of Theorem 4.1 does not depend on the fluid-solid density ratio neither on the geometry of the domain, the semi-implicit coupling scheme* (24)-(26) *remains stable irrespectively of the added-mass effect. This was not the case of the original semi-implicit scheme reported in [14] (see condition* (1)*). Moreover, thanks to the natural interface dissipation of the Robin coupling, diffusive time marching in the structure is no longer needed to ensure stability. As a matter of fact, here we have considered a conservative scheme (see the energy equation* (29)*). We emphasize that this was not the case for the original semi-implicit scheme (see [14, Remarks 3,4]).*

Remark 4.3 *The extra dissipative interface term* $\gamma\mu\tau/(2h)\|\tilde{\boldsymbol{u}}_h^n\|_{0,\Sigma}^2$ *in* (27) *and the CFL-like condition* $\gamma\mu\tau = \mathcal{O}(h)$ *arise also in the Nitsche based stabilized explicit coupling reported in [8]. On the contrary, here we do not need to stabilize pressure fluctuations, that is, to introduce a weakly consistent artificial compressibility at the interface. Indeed, due to the implicit treatment of the pressure-solid coupling, no artificial pressure power appears in the energy estimate* (30)*.*

Remark 4.4 *One can prove a similar energy estimate for the pressure-correction version of algorithm* (24)-(26)*. Indeed, under the same assumptions as in Theorem 4.1, there holds*

$$E^n + \mu\tau \sum_{m=0}^{n-1} \|\boldsymbol{\epsilon}(\tilde{\boldsymbol{u}}_h^{m+1})\|_{0,\Omega^{\mathrm{f}}}^2 + (\gamma - 2C_{\mathrm{ti}})\frac{\mu\tau}{2h}\sum_{m=0}^{n}\|\tilde{\boldsymbol{u}}_h^{m+1} - D_\tau \boldsymbol{d}_H^{m+1}\|_{0,\Sigma}^2 + \frac{\gamma\mu\tau}{2h}\|D_\tau \boldsymbol{d}_H^n\|_{0,\Sigma}^2 \leq E^0 + \mu\tau\|\boldsymbol{\epsilon}(\tilde{\boldsymbol{u}}_h^0)\|_{0,\Omega^{\mathrm{f}}}^2 + \frac{\gamma\mu\tau}{2h}\|D_\tau \boldsymbol{d}_H^0\|_{0,\Sigma}^2.$$

Note that, in this case, the extra numerical dissipation (mentioned in the previous remark) appears in the solid-side, that is $\gamma\mu\tau/(2h)\|D_\tau \boldsymbol{d}_H^n\|_{0,\Sigma}^2$*.*

4.3 Semi-Implicit Coupling With Pressure-Poisson Formulation

The pressure-Poisson version of Algorithm 1 (see §3.4.1) applied to the model problem (23) reads:

- Implicit step (pressure-solid coupling):
  Find $(p_h^{n+1}, \boldsymbol{u}_h^{n+1}, \boldsymbol{d}_H^{n+1}, \dot{\boldsymbol{d}}_H^{n+1}) \in Q_h^{\mathrm{f}} \times V_h^{\mathrm{f}} \times [V_H^{\mathrm{s}}]^2$ such that

$$\begin{cases} (\boldsymbol{\nabla} p_h^{n+1}, \boldsymbol{\nabla} q_h)_{\Omega^{\mathrm{f}}} = -\dfrac{\rho^{\mathrm{f}}}{\tau}(\boldsymbol{\nabla}\cdot\tilde{\boldsymbol{u}}_h^n, q_h)_{\Omega^{\mathrm{f}}} \\ \qquad\qquad\qquad\qquad - \dfrac{\rho^{\mathrm{f}}}{\tau}\big((\pi_h(D_\tau \boldsymbol{d}_H^{n+1}) - \tilde{\boldsymbol{u}}_h^n)\cdot\boldsymbol{n}^{\mathrm{f}}, q_h\big)_\Sigma \quad \forall q_h \in Q_{\Gamma,h}^{\mathrm{f}}, \\ \qquad\qquad\qquad\qquad\qquad\qquad p_h^{n+1} = \bar{p} \quad \text{on} \quad \Gamma^{\mathrm{in-out}}. \end{cases} \tag{34}$$

$$\begin{cases} \dfrac{\rho^{\mathrm{f}}}{\tau}\big(\boldsymbol{u}_h^{n+1} - \tilde{\boldsymbol{u}}_h^n, \boldsymbol{v}_h^{\mathrm{f}}\big)_{\Omega^{\mathrm{f}}} + \big(\boldsymbol{\nabla} p_h^{n+1}, \boldsymbol{v}_h^{\mathrm{f}}\big)_{\Omega^{\mathrm{f}}} = 0 \quad \forall \boldsymbol{v}_h^{\mathrm{f}} \in V_{\Sigma,h}^{\mathrm{f}}, \\ \qquad\qquad\qquad\qquad \boldsymbol{u}_h^{n+1} = \pi_h(D_\tau \boldsymbol{d}_H^{n+1}) \quad \text{on} \quad \Sigma. \end{cases} \tag{35}$$

$$\begin{cases} \dfrac{\rho^{\mathrm{s}}}{\tau}\big(\dot{\boldsymbol{d}}_H^{n+1} - \dot{\boldsymbol{d}}_H^n, \boldsymbol{v}_H^{\mathrm{s}}\big)_{\Omega^{\mathrm{s}}} + a^{\mathrm{s}}\big(\boldsymbol{d}_H^{n+\frac{1}{2}}, \boldsymbol{v}_H^{\mathrm{s}}\big) + \dfrac{\gamma\mu}{h}\big(\pi_h(D_\tau \boldsymbol{d}_H^{n+1}) - \tilde{\boldsymbol{u}}_h^n, \pi_h(\boldsymbol{v}_H^{\mathrm{s}})\big)_\Sigma \\ \qquad = -2\mu\big(\boldsymbol{\epsilon}(\tilde{\boldsymbol{u}}_h^n)\boldsymbol{n}^{\mathrm{s}}, \pi_h(\boldsymbol{v}_H^{\mathrm{s}})\big)_\Sigma - \big\langle \mathcal{R}(\boldsymbol{u}_h^{n+1}, \tilde{\boldsymbol{u}}_h^n, p_h^{n+1}), \mathcal{L}_h(\boldsymbol{v}_H^s)\big\rangle \quad \forall \boldsymbol{v}_H^{\mathrm{s}} \in V_H^{\mathrm{s}}, \\ \qquad\qquad\qquad\qquad D_\tau \boldsymbol{d}_H^{n+1} = \dot{\boldsymbol{d}}_H^{n+\frac{1}{2}} \quad \text{in} \quad \Omega^{\mathrm{s}}. \end{cases} \tag{36}$$

- Explicit step (viscous-solid coupling):
  Find $\tilde{\boldsymbol{u}}_h^{n+1} \in V_h^{\mathrm{f}}$ such that

$$\left\{ \begin{array}{r} \dfrac{\rho^{\mathrm{f}}}{\tau}\big(\tilde{\boldsymbol{u}}_h^{n+1} - \boldsymbol{u}_h^{n+1}, \tilde{\boldsymbol{v}}_h^{\mathrm{f}}\big)_{\Omega^{\mathrm{f}}} + 2\mu\big(\boldsymbol{\epsilon}(\tilde{\boldsymbol{u}}_h^{n+1}), \boldsymbol{\epsilon}(\tilde{\boldsymbol{v}}_h^{\mathrm{f}})\big)_{\Omega^{\mathrm{f}}} + \dfrac{\gamma\mu}{h}\big(\tilde{\boldsymbol{u}}_h^{n+1} - \pi_h(D_\tau \boldsymbol{d}_H^{n+1}), \tilde{\boldsymbol{v}}_h^{\mathrm{f}}\big)_\Sigma \\ = 2\mu\big(\boldsymbol{\epsilon}(\tilde{\boldsymbol{u}}_h^n)\boldsymbol{n}^{\mathrm{f}}, \tilde{\boldsymbol{v}}_h^{\mathrm{f}}\big)_\Sigma \quad \forall \tilde{\boldsymbol{v}}_h^{\mathrm{f}} \in V_h^{\mathrm{f}}. \end{array} \right. \tag{37}$$

4.3.1 Energy Based Stability Analysis

In this subsection, we provide an energy based estimate for the semi-implicit scheme (34)-(37) involving a pressure-Poisson equation.

In the analysis below, we shall make use of the following result (whose proof can be found in Appendix), allowing to reformulate (34)-(35) as the Darcy-like problem, but with a modified continuity equation.

Lemma 4.5 *Assume that* (34)-(35) *holds. Then*

$$-(q_h, \boldsymbol{\nabla}\cdot \boldsymbol{u}_h^{n+1})_{\Omega^{\mathrm{f}}} = \frac{\tau}{\rho^{\mathrm{f}}}(\boldsymbol{\nabla} q_h, \Pi_h^\perp(\boldsymbol{\nabla} p_h^{n+1}))_{\Omega^{\mathrm{f}}} - (\boldsymbol{\nabla} q_h, \Pi_h^\perp(\tilde{\boldsymbol{u}}_h^n - \mathcal{L}_h(D_\tau \boldsymbol{d}_H^{n+1})))_{\Omega^{\mathrm{f}}}$$

for all $q_h \in Q_{\Gamma,h}^{\mathrm{f}}$. *Here,* $\Pi_h : L^2(\Omega^{\mathrm{f}}) \to V_{\Sigma,h}^{\mathrm{f}}$ *stands for the* L^2*-projection operator into* $V_{\Sigma,h}^{\mathrm{f}}$, *and* $\Pi_h^\perp \overset{\mathrm{def}}{=} I - \Pi_h$ *for the corresponding orthogonal projection.*

We now state the main result of this subsection, which provides the conditional stability of the coupling scheme (34)-(37).

Theorem 4.6 *Assume that* (16) *holds and that the system is isolated, i.e.* $\bar{p} = 0$ *on* $\Gamma^{\mathrm{in-out}}$. *Let* $\big\{(\tilde{\boldsymbol{u}}_h^n, \boldsymbol{u}_h^n, p_h^n, \boldsymbol{d}_H^n, \dot{\boldsymbol{d}}_H^n)\big\}_{n\geq 0}$ *be solution of* (34)-(37). *Then, the following discrete energy estimate holds:*

$$\begin{aligned} E^n + \mu\tau \sum_{m=0}^{n-1} \|\boldsymbol{\epsilon}(\tilde{\boldsymbol{u}}_h^{m+1})\|_{0,\Omega^{\mathrm{f}}}^2 + \frac{\tau^2}{2\rho^{\mathrm{f}}} \sum_{m=0}^{n-1} ||\Pi_h^\perp(\boldsymbol{\nabla} p_h^{m+1})||_{0,\Omega^{\mathrm{f}}}^2 \\ + \frac{\mu\tau}{4h}\left(\gamma - 4C_{\mathrm{ti}} - \frac{4C_{\mathcal{L}}\rho^{\mathrm{f}}h^2}{\mu\tau}\right) \sum_{m=0}^{n-1} \|\tilde{\boldsymbol{u}}_h^{m+1} - \pi_h(D_\tau \boldsymbol{d}_H^{m+1})\|_{0,\Sigma}^2 \\ + \frac{\gamma\mu\tau}{2h}\|\tilde{\boldsymbol{u}}_h^n\|_{0,\Sigma}^2 + \frac{\mu\tau}{6h}\left(\gamma - \frac{6C_{\mathcal{L}}\rho^{\mathrm{f}}h^2}{\mu\tau}\right) \sum_{m=0}^{n-1} \|\tilde{\boldsymbol{u}}_h^{m+1} - \tilde{\boldsymbol{u}}_h^m\|_{0,\Sigma}^2 \\ \leq E^0 + \mu\tau\|\boldsymbol{\epsilon}(\tilde{\boldsymbol{u}}_h^0)\|_{0,\Omega^{\mathrm{f}}}^2 + \frac{\gamma\mu\tau}{2h}\|\tilde{\boldsymbol{u}}_h^0\|_{0,\Sigma}^2. \end{aligned} \tag{38}$$

Thus, the semi-implicit coupling scheme (34)-(37) *is stable, in the energy norm, under the conditions:*

$$\gamma \geq 8C_{\mathrm{ti}}, \quad \gamma\mu\tau = \mathcal{O}(h), \quad \gamma\mu\tau \geq 8\rho^{\mathrm{f}} C_{\mathcal{L}} h^2. \tag{39}$$

Proof. As in Theorem 4.1, we take in (34)-(37)

$$\boldsymbol{v}_h^{\mathrm{f}} = \tau(\boldsymbol{u}_h^{n+1} - \mathcal{L}_h(D_\tau \boldsymbol{d}_H^{n+1})), \quad q_h = \tau p_h^{n+1}, \quad \boldsymbol{v}_H^{\mathrm{s}} = \tau D_\tau \boldsymbol{d}_H^{n+1}, \quad \tilde{\boldsymbol{v}}_h^{\mathrm{f}} = \tau \tilde{\boldsymbol{u}}_h^{n+1}$$

and we sum the resulting expressions to obtain

$$E^{n+1} - E^n + 2\mu\tau\|\boldsymbol{\epsilon}(\tilde{\boldsymbol{u}}_h^{n+1})\|_{0,\Omega^{\mathrm{f}}}^2 \underbrace{-2\mu\tau\big(\boldsymbol{\epsilon}(\tilde{\boldsymbol{u}}_h^n)\boldsymbol{n}^{\mathrm{f}}, \tilde{\boldsymbol{u}}_h^{n+1} - \pi_h(D_\tau \boldsymbol{d}_H^{n+1})\big)_\Sigma}_{\mathcal{T}_2}$$
$$+ \underbrace{\frac{\gamma\mu\tau}{h}\big[\big(\pi_h(D_\tau \boldsymbol{d}_H^{n+1}) - \tilde{\boldsymbol{u}}_h^n, \pi_h(D_\tau \boldsymbol{d}_H^{n+1})\big)_\Sigma + \big(\tilde{\boldsymbol{u}}_h^{n+1} - \pi_h(D_\tau \boldsymbol{d}_H^{n+1}), \tilde{\boldsymbol{u}}_h^{n+1}\big)_\Sigma\big]}_{\mathcal{T}_1}$$
$$\underbrace{-\tau(p_h^{n+1}, \boldsymbol{\nabla}\cdot\boldsymbol{u}_h^{n+1})_{\Omega^{\mathrm{f}}}}_{\mathcal{T}_3} \leq 0. \quad (40)$$

Terms $\mathcal{T}_1$ and $\mathcal{T}_2$ can be bounded using arguments similar to those used in the proof of Theorem 4.1. Nevertheless, the new term $\mathcal{T}_3$ requires a specific treatment of term $\mathcal{T}_1$ as we shall see below.

Let consider first term $\mathcal{T}_3$. Using Lemma 4.5, the L^2-orthogonality of Π_h and the Cauchy-Schwarz inequality, we have that

$$\begin{aligned}
\mathcal{T}_3 =& \frac{\tau^2}{\rho^{\mathrm{f}}}(\boldsymbol{\nabla} p_h^{n+1}, \Pi_h^\perp(\boldsymbol{\nabla} p_h^{n+1}))_{\Omega^{\mathrm{f}}} - \tau(\boldsymbol{\nabla} p_h^{n+1}, \Pi_h^\perp(\tilde{\boldsymbol{u}}_h^n - \mathcal{L}_h(D_\tau \boldsymbol{d}_H^{n+1})))_{\Omega^{\mathrm{f}}} \\
=& \frac{\tau^2}{\rho^{\mathrm{f}}}\|\Pi_h^\perp(\boldsymbol{\nabla} p_h^{n+1})\|_{0,\Omega^{\mathrm{f}}}^2 - \tau(\Pi_h^\perp(\boldsymbol{\nabla} p_h^{n+1}), \Pi_h^\perp(\tilde{\boldsymbol{u}}_h^n - \mathcal{L}_h(D_\tau \boldsymbol{d}_H^{n+1})))_{\Omega^{\mathrm{f}}} \quad (41) \\
\geq& \frac{\tau^2}{2\rho^{\mathrm{f}}}\|\Pi_h^\perp(\boldsymbol{\nabla} p_h^{n+1})\|_{0,\Omega^{\mathrm{f}}}^2 - \frac{\rho^{\mathrm{f}}}{2}\|\Pi_h^\perp(\tilde{\boldsymbol{u}}_h^n - \mathcal{L}_h(D_\tau \boldsymbol{d}_H^{n+1}))\|_{0,\Omega^{\mathrm{f}}}^2.
\end{aligned}$$

In order to bound the last term, we note that

$$\tilde{\boldsymbol{u}}_h^n - \mathcal{L}_h(D_\tau \boldsymbol{d}_H^{n+1}) = \tilde{\boldsymbol{u}}_h^n - \mathcal{L}_h^{\mathrm{f}}(\tilde{\boldsymbol{u}}_h^n) + \mathcal{L}_h^{\mathrm{f}}(\tilde{\boldsymbol{u}}_h^n) - \mathcal{L}_h^{\mathrm{f}}\big(\pi_h(D_\tau \boldsymbol{d}_H^{n+1})\big),$$

and since $\tilde{\boldsymbol{u}}_h^n - \mathcal{L}_h^{\mathrm{f}}(\tilde{\boldsymbol{u}}_h^n) \in V_{\Sigma,h}^{\mathrm{f}}$ (by construction), we have that

$$\|\Pi_h^\perp(\tilde{\boldsymbol{u}}_h^n - \mathcal{L}_h(D_\tau \boldsymbol{d}_H^{n+1}))\|_{0,\Omega^{\mathrm{f}}}^2 = \|\Pi_h^\perp \mathcal{L}_h^{\mathrm{f}}(\tilde{\boldsymbol{u}}_h^n - \pi_h(D_\tau \boldsymbol{d}_H^{n+1}))\|_{0,\Omega^{\mathrm{f}}}^2. \quad (42)$$

On the other hand, thanks to the L^2-continuity estimate (16), it follows that

$$\begin{aligned}
\|\Pi_h^\perp \mathcal{L}_h^{\mathrm{f}}(\tilde{\boldsymbol{u}}_h^n - \pi_h(D_\tau \boldsymbol{d}_H^{n+1}))\|_{0,\Omega^{\mathrm{f}}}^2 \leq& \|\mathcal{L}_h^{\mathrm{f}}(\tilde{\boldsymbol{u}}_h^n - \pi_h(D_\tau \boldsymbol{d}_H^{n+1}))\|_{0,\Omega^{\mathrm{f}}}^2 \\
\leq& C_{\mathcal{L}} h\|\tilde{\boldsymbol{u}}_h^n - \pi_h(D_\tau \boldsymbol{d}_H^{n+1})\|_{0,\Sigma}^2 \\
\leq& 2C_{\mathcal{L}} h\big(\|\tilde{\boldsymbol{u}}_h^n - \tilde{\boldsymbol{u}}_h^{n+1}\|_{0,\Sigma}^2 \\
&+ \|\tilde{\boldsymbol{u}}_h^{n+1} - \pi_h(D_\tau \boldsymbol{d}_H^{n+1})\|_{0,\Sigma}^2\big).
\end{aligned} \quad (43)$$

In summary, from (41)-(43), we conclude that

$$\mathcal{T}_3 \geq \frac{\tau^2}{2\rho^{\mathrm{f}}}\|\Pi_h^\perp(\boldsymbol{\nabla} p_h^{n+1})\|_{0,\Omega^{\mathrm{f}}}^2 - C_{\mathcal{L}}\rho^{\mathrm{f}} h\big(\|\tilde{\boldsymbol{u}}_h^n - \tilde{\boldsymbol{u}}_h^{n+1}\|_{0,\Sigma}^2 + \|\tilde{\boldsymbol{u}}_h^{n+1} - \pi_h(D_\tau \boldsymbol{d}_H^{n+1})\|_{0,\Sigma}^2\big). \quad (44)$$

The first term in the last inequality corresponds to the well known enhanced pressure stability of the Chorin-Temam scheme in a pressure-Poisson formulation. The last term will be controlled using the natural numerical dissipation provided by term $\mathcal{T}_1$.

As in the proof of Theorem 4.1, we have

$$\mathcal{T}_1 = \frac{\gamma\mu\tau}{h}\left[\|\tilde{\boldsymbol{u}}_h^{n+1} - \pi_h(D_\tau \boldsymbol{d}_H^{n+1})\|_{0,\Sigma}^2 + \left(\tilde{\boldsymbol{u}}_h^{n+1} - \tilde{\boldsymbol{u}}_h^n, \pi_h(D_\tau \boldsymbol{d}_H^{n+1})\right)_\Sigma\right], \quad (45)$$

and, using Young's inequality,

$$\begin{aligned}\left(\tilde{\boldsymbol{u}}_h^{n+1} - \tilde{\boldsymbol{u}}_h^n, \pi_h(D_\tau \boldsymbol{d}_H^{n+1})\right)_\Sigma =& \left(\tilde{\boldsymbol{u}}_h^{n+1} - \tilde{\boldsymbol{u}}_h^n, \pi_h(D_\tau \boldsymbol{d}_H^{n+1}) - \tilde{\boldsymbol{u}}_h^{n+1}\right)_\Sigma + \left(\tilde{\boldsymbol{u}}_h^{n+1} - \tilde{\boldsymbol{u}}_h^n, \tilde{\boldsymbol{u}}_h^{n+1}\right)_\Sigma \\ \geq& -\frac{1}{2\varepsilon}\|\tilde{\boldsymbol{u}}_h^{n+1} - \tilde{\boldsymbol{u}}_h^n\|_{0,\Sigma}^2 - \frac{\varepsilon}{2}\|\pi_h(D_\tau \boldsymbol{d}_H^{n+1}) - \tilde{\boldsymbol{u}}_h^{n+1}\|_{0,\Sigma}^2 \\ &+ \frac{1}{2}\|\tilde{\boldsymbol{u}}_h^{n+1}\|_{0,\Sigma}^2 - \frac{1}{2}\|\tilde{\boldsymbol{u}}_h^n\|_{0,\Sigma}^2 + \frac{1}{2}\|\tilde{\boldsymbol{u}}_h^{n+1} - \tilde{\boldsymbol{u}}_h^n\|_{0,\Sigma}^2 \\ \geq& -\frac{\varepsilon}{2}\|\pi_h(D_\tau \boldsymbol{d}_H^{n+1}) - \tilde{\boldsymbol{u}}_h^{n+1}\|_{0,\Sigma}^2 + \left(\frac{1}{2} - \frac{1}{2\varepsilon}\right)\|\tilde{\boldsymbol{u}}_h^{n+1} - \tilde{\boldsymbol{u}}_h^n\|_{0,\Sigma}^2 \\ &+ \frac{1}{2}\|\tilde{\boldsymbol{u}}_h^{n+1}\|_{0,\Sigma}^2 - \frac{1}{2}\|\tilde{\boldsymbol{u}}_h^n\|_{0,\Sigma}^2, \end{aligned} \quad (46)$$

with $\varepsilon > 0$ arbitrary. Therefore, chosing $\varepsilon = \frac{3}{2}$ in (46) and inserting the resulting estimate in (45) yields

$$\mathcal{T}_1 \geq \frac{\gamma\mu\tau}{h}\left[\frac{1}{4}\|\tilde{\boldsymbol{u}}_h^{n+1} - \pi_h(D_\tau \boldsymbol{d}_H^{n+1})\|_{0,\Sigma}^2 + \frac{1}{6}\|\tilde{\boldsymbol{u}}_h^{n+1} - \tilde{\boldsymbol{u}}_h^n\|_{0,\Sigma}^2 + \frac{1}{2}\|\tilde{\boldsymbol{u}}_h^{n+1}\|_{0,\Sigma}^2 - \frac{1}{2}\|\tilde{\boldsymbol{u}}_h^n\|_{0,\Sigma}^2\right]. \quad (47)$$

On the other hand, similarly to (33), we have

$$\mathcal{T}_2 \geq -\mu\tau\|\boldsymbol{\epsilon}(\tilde{\boldsymbol{u}}_h^n)\|_{0,\Omega^{\mathrm{f}}}^2 - \frac{\mu\tau C_{\mathrm{ti}}}{h}\|\tilde{\boldsymbol{u}}_h^{n+1} - \pi_h(D_\tau \boldsymbol{d}_H^{n+1})\|_{0,\Sigma}^2. \quad (48)$$

Finally, by inserting in (40) the estimates (44), (47) and (48), changing n by m and summing over $m = 0, \ldots, n-1$, we obtain (38), which completes the proof.

Remark 4.7 *The stability condition* (39)*, for the pressure-Poisson formulation, is stronger than condition* (28)*, for the pressure-Darcy formulation. Note that* (39) *enforces a restriction on the rate with which h and τ go to zero, namely, $h^2 = O(\tau)$. It is interesting to observe that this restriction arises also in the case of equal order velocity-pressure approximations of the Chorin-Temam scheme (for a pure fluid problem) with a pressure-Poisson equation (see e.g. [3, Assumption 8]). Obviously, condition $h^2 = O(\tau)$ is compatible with $\gamma\tau\mu = O(h)$.*

Remark 4.8 *Although* (39) *depends on the physical parameters ρ^{f} and μ, the scheme is still stable irrespectively of the amount of added-mass effect. Finally, we remark that the considered numerical experiments showed that this dependence do not affect the stability of the scheme.*

5 Numerical Experiments

In order to illustrate the stability and accuracy properties of the coupling schemes, different numerical experiments are discussed. In subsection §5.1 we report two different numerical tests involving the Stokes-linear elasticity coupling (23) in 2D. The non-linear case (2)-(3), with more realistic 3D geometries, is considered in subsection §5.2. In all cases, we have considered fluid-solid space discretizations matching at the interface.

5.1 Two-Dimensional Test-Cases

We have considered both the pressure-Poisson and pressure-Darcy versions of our scheme, with a FWI-based pressure stress computation. The implicit part of the coupling has been solved using Aitken's accelerated fixed-point iterations (see e.g. [24]). The numerical computations have been carried out with Freefem++ [23].

5.1.1 An Analytical Test-Case

We approximate an analytical solution of the Stokes-linear elasticity coupling:

$$\begin{cases} p(x,y) = [-2L_2\cos(\pi t)/\pi - 2\mu\sin(\pi t)]\sin(x)\sin(y), \\ \boldsymbol{u}(x,y) = \big(-\sin(\pi t)\cos(x)\sin(y), \sin(\pi t)\sin(x)\cos(y)\big), \\ \boldsymbol{d}(x,y) = \big(\cos(\pi t)\cos(x)\sin(y)/\pi, -\cos(\pi t)\sin(x)\cos(y)/\pi\big), \end{cases}$$

where L_2 stands for the second Lamé constant of the solid. The fluid and solid domains, reported in Figure 2 (left), are given by $\Omega^{\mathrm{f}} = [0,\pi]\times[0,\pi]$ and $\Omega^{\mathrm{s}} = [0,\pi]\times[\pi,1.25\pi]$. Initial conditions, external boundary conditions and the

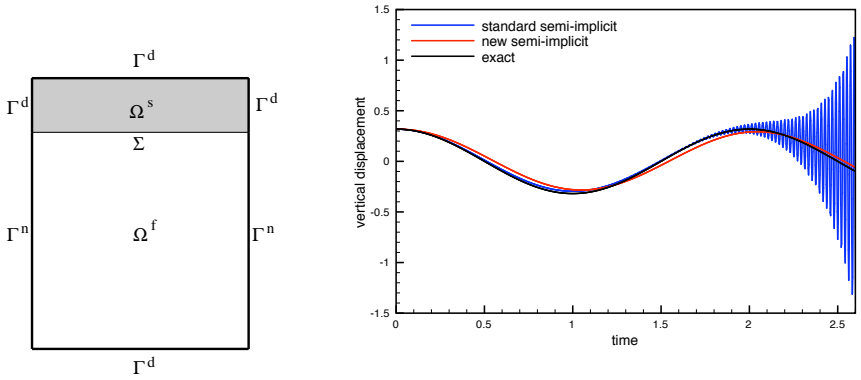

Figure 2: Left: Computational domain. Right: comparison of the semi-implicit and the Robin based semi-implicit coupling schemes (interface mid-point vertical displacement).

body forces, both for the fluid and the structure, are chosen in order to satisfy the exact solution. In particular, Dirichlet and Neumann boundary conditions are respectively imposed on Γ^{d} and Γ^{n} for both the problems. The physical parameters are $\rho^{\mathrm{f}} = 1.0$ g/cm^3, $\mu = 4$ poise, $\rho^{\mathrm{s}} = 2.15$ g/cm^3, the elastic modulus $E = 1$ dyne/cm^2, and the Poisson's ratio $\nu = 0.3$.

The pressure-Poisson version of Algorithm 1 and the original semi-implicit coupling [14] are tested using $\mathbb{P}_1$ finite elements. The penalty parameter γ has been fixed to 10. The mesh size is $h = \pi/20$ and the time step is $\tau = 2.5\times10^{-3}$ s. Strong instabilities are observed for the original semi-implicit coupling scheme, see Figure 2 (right). On the contrary, our Robin based semi-implicit coupling scheme is stable and predicts the behavior of the exact solution.

5.1.2 Pressure Wave Propagation in a Compliant Vessel

We consider the 2D test-case already used in [8, Section 6.1]. The fluid domain is given by $\Omega^{\mathrm{f}} \overset{\mathrm{def}}{=} [0,5] \times [0,0.5]$ and the solid domain by $\Omega^{\mathrm{s}} \overset{\mathrm{def}}{=} [0,5] \times [0.5,0.6]$. At $x = 0$, we impose a pressure of value $P = 10^4$ dyne/cm^2, during 5×10^{-3} s. Zero pressure is enforced at $x = 5$. A symmetry condition is applied on the lower wall $y = 0$. The structure is clamped on $x = 0$ and $x = 5$, with zero traction applied on $y = 0.6$. The fluid physical parameters are given by $\rho^{\mathrm{f}} = 1.0$ g/cm^3, $\mu = 10$ poise. For the solid, we have $\rho^{\mathrm{s}} = 1.2 \times 10^{-2}$ g/cm^3, the elastic modulus $E = 3 \times 10^8$ dyne/cm^2, and the Poisson's ratio $\nu = 0.3$. Note that these values (high viscosity and small solid density) have been chosen so that the stability condition (1), for the original semi-implicit coupling scheme, is expected not to be satisfied. For the fluid, we used the Taylor-Hood finite element and for the structure a standard $\mathbb{P}_1$-continuous discretization with mesh sizes of $h = 0.1$. The time step was fixed to $\tau = 10^{-4}$ s. The penalty parameter γ is still fixed to 10.

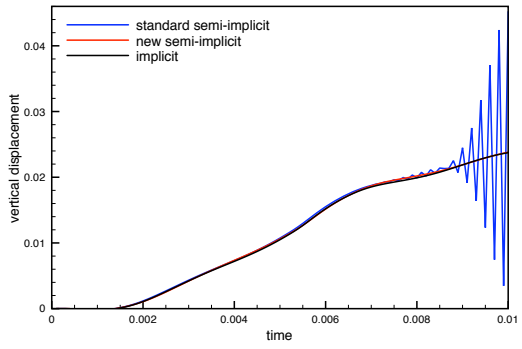

Figure 3: Comparison of the semi-implicit and Robin based semi-implicit coupling schemes: interface mid-point vertical displacement.

A comparison between our Robin based semi-implicit coupling, in its pressure-Darcy version, an implicit coupling and the original semi-implicit coupling [14] is given in Figure 3. Strong numerical instabilities are observed for the latter strategy. However, Algorithm 1 provides a stable numerical solution which accurately predicts the results of the fully implicit coupling. Simulations have been also carried out with the pressure-Poisson version of the algorithm, with the same results as in pressure-Darcy version.

5.2 Three-Dimensional Test-Cases

Here we have considered the pressure-Poisson version of Algorithm 1. The implicit coupling step is solved using a partitioned Dirichlet-Neumann interface Newton-GMRES algorithm, as in [14]. Comparisons are made with a reference solution obtained with a fully implicit scheme (solved through a partitioned Dirichlet-Neumann interface Newton-GMRES algorithm, see e.g. [15]). The LifeV[1] finite element library has been used for the numerical computations.

[1] WWW.LIFEV.ORG

5.2.1 Pressure Wave Progation in a Straight Cylindrical Vessel

In order to investigate the properties of the algorithm in its non-linear version we considered three-dimensional benchmark proposed in [16] (see also [17, Chapter 12]). The fluid domain is a straight tube of radius 0.5 cm and of length 5 cm. The fluid is governed by the incompressible Navier-Stokes equations in ALE formulation. The vessel wall has a thickness of 0.1 cm and is clamped at its extremities. Here, we assume that the vessel displacement is governed by the laws of linear elasticity. The physical parameters for the fluid have been chosen as $\rho^{\mathrm{f}} = 1$ g/cm^3 and $\mu = 0.035$ poise. For the solid we have $\rho^{\mathrm{s}} = 1.2$ g/cm^3, Young modulus $E = 3 \times 10^6$ dynes/cm^2 and Poisson's ratio $\nu = 0.3$. The overall system is initially at rest and, during the first 5×10^{-3} seconds, an over pressure of 1.3332×10^4 dynes/cm^2 is imposed on the inlet boundary.

The penalty parameter γ has been fixed to 50. $\mathbb{P}_1/\mathbb{P}_1$-continuous finite elements, with SUPG stabilization (see e.g. [33]), have been chosen for discretization in space of the fluid and $\mathbb{P}_1$-continuous finite elements for discretization of the solid. Simulations are carried out on 400 time steps of length $\tau = 10^{-4}$ seconds.

Figure 4 shows the fluid pressure and the solid deformation at different time instants. A stable pressure wave propagation is observed, both for the standard and the new semi-implicit schemes. Moreover, the maximum displacement has been computed and compared to a reference simulation obtained with a full implicit coupling scheme. The results are displayed in Figure 5. Both the standard and the Robin based semi-implicit coupling schemes provide a stable prediction that compares well to the reference implicit solution.

Table 5.2.1 shows the computational time of the different methods, for 400 time steps. Standard and Robin based semi-implicit coupling schemes are comparable in terms of computation time, and are more than 6 times faster than the traditional implicit coupling. As a result, the good computational performance of the original semi-implicit scheme is conserved by our Robin based scheme. Note finally that in the version FWI, the algorithm is twice as fast as in the version VR. The difference is explained of course by the computation of the variational residual, which increases the computational cost.

Algorithm	CPU Time
Implicit	13.1
Standard semi-implicit (VR/FWI)	1.9/0.9
New semi-implicit (VR/FWI)	2.0/1.0

Table 1: Elapsed CPU Time (dimensionless)

5.2.2 A Physiological Test-Case

We consider now the numerical fluid-structure simulations reported in [28] using *in vitro* aneurysm geometries. The fluid computational domain is the idealized abdominal aortic aneurysm given in Figure 6 (left). We refer to [28, 29] for the details. The whole compliant wall has a uniform thickness of 0.17 cm and length of 22.95 cm.

The physical parameters are given by $E = 6 \times 10^6\,\mathrm{dynes/cm^2}$, $\nu = 0.3$, $\rho^{\mathrm{s}} = 1.2\,\mathrm{g/cm^3}$, $\mu = 0.035\,\mathrm{poise}$ and $\rho^{\mathrm{f}} = 1\,\mathrm{g/cm^2}$. Initially, the fluid is at rest.

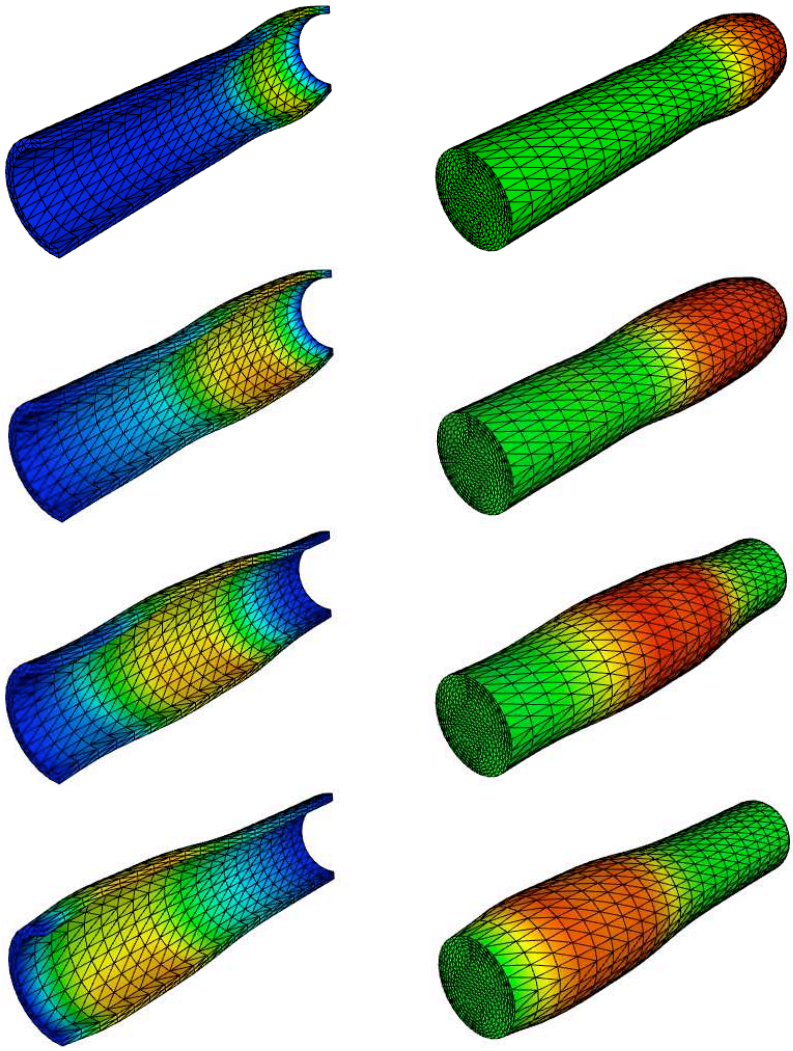

Figure 4: Robin based semi-implicit coupling: snapshots of the - exaggerated - solid deformation and of the pressure at different time instants ($t = 0.0025$, 0.005, 0.0075 and 0.01 seconds).

An in-flow rate corresponding to a cardiac cycle, see Figure 6(right), is imposed on the inlet boundary. A resistive-like boundary condition is prescribed on the outlet boundary, the value of the resistance being $R = 6 \times 10^2\,\mathrm{dyne/cm^3}$.

As regards the discretization in space, $\mathbb{P}_1/\mathbb{P}_1$-continuous finite elements, with SUPG stabilization, have been chosen for the fluid and $\mathbb{P}_1$-continuous finite elements for the solid. The penalty parameter γ has been fixed to 50. We have simulated 1000 time steps of length $\tau = 1.68 \times 10^{-3}\,\mathrm{s}$, which corresponds to two cardiac cycles.

In Figure 7, we have reported some snapshots of the wall deformation and the fluid velocity fields at different time instants. In Figure 8, it is shown that

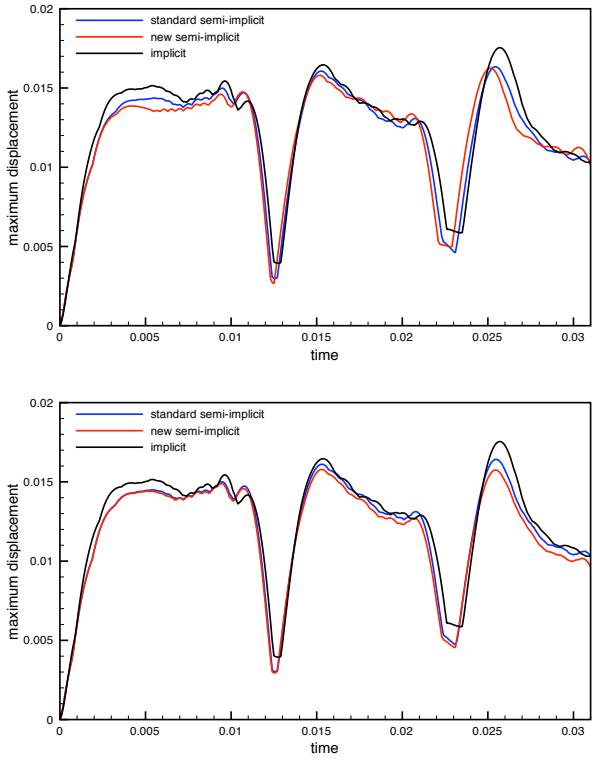

Figure 5: Comparison of the implicit, standard semi-implicit and Robin based semi-implicit coupling schemes: maximal displacement of the structure. Top: VR. Bottom: FWI.

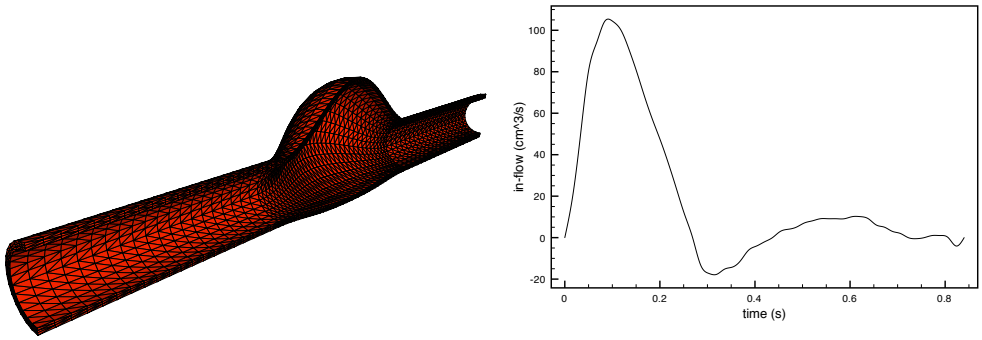

Figure 6: Aneurysm geometry (left) and in-flow rate data (right)

even in this complex case, the standard and Robin based semi-implicit coupling provide a prediction that compares well to the reference implicit solution.

In table 2, we have reported the CPU-time consumption over 500 time steps (two full cardiac cycles), for the different methods considered. Again, the standard and Robin based semi-implicit schemes are comparable in terms of com-

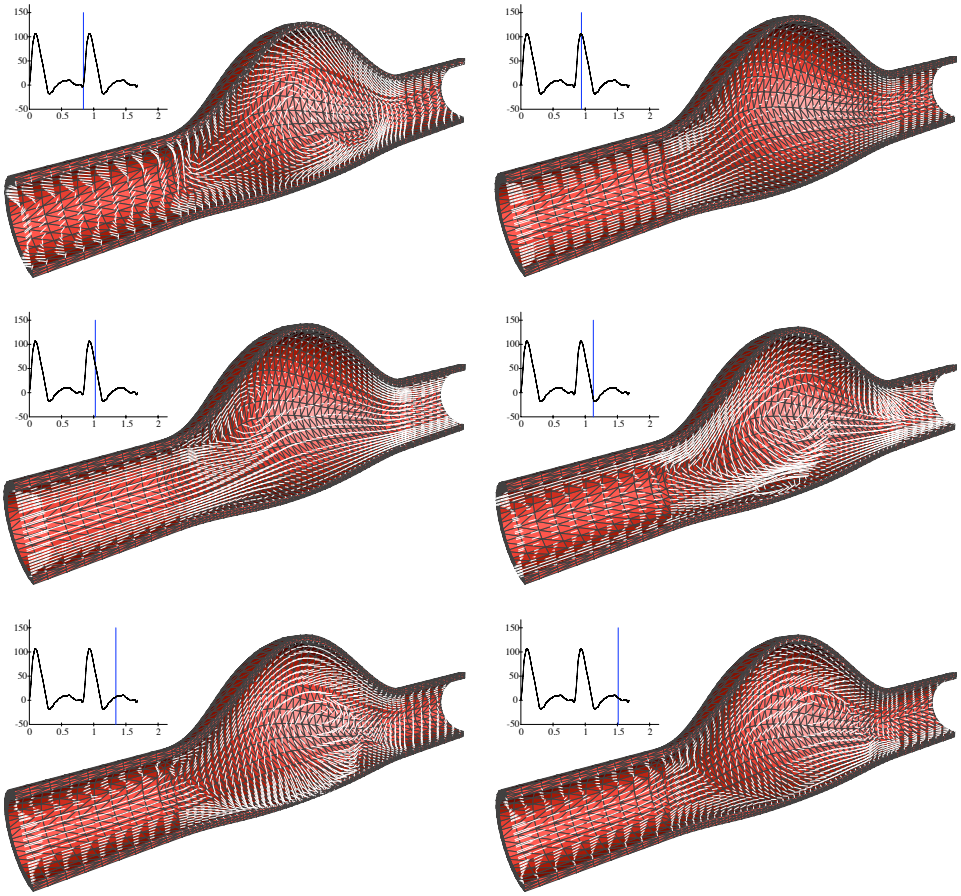

Figure 7: Robin based semi-implicit coupling: snapshots of the solid deformation and fluid velocity field at different time instants.

putational cost. They are more than 10 times faster than the classical fully implicit algorithm.

Algorithm	CPU Time
Implicit	16.4
Standard semi-implicit (VR/FWI)	1.5/1.1
New semi-implicit (VR/FWI)	1.4/ 1

Table 2: Elapsed CPU Time (dimensionless)

6 Conclusion

We have proposed a Robin-based semi-implicit coupling scheme whose stability properties are independent of:

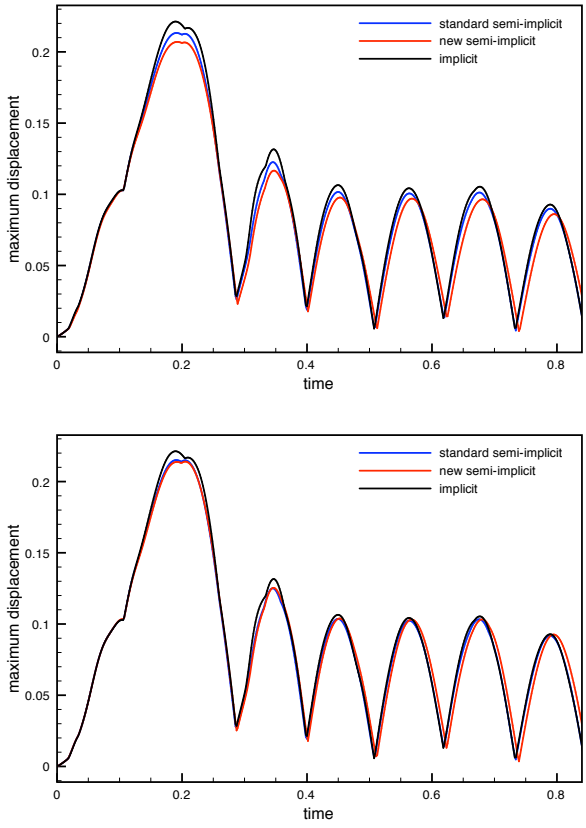

Figure 8: Comparison of the implicit, standard semi-implicit and Robin based semi-implicit coupling schemes: maximal displacement of the structure. Top: VR. Bottom: FWI.

1. the added-mass effect in the system (fluid-solid density ratio and geometry of the domain);
2. the numerical dissipation of the solid time-discretization.

In particular, it allows for conservative time-stepping on the structure without compromising stability. The main idea consists in treating the explicit part of the coupling with a Robin based mortaring derived from Nitsche's method. Numerical tests confirm the theoretical results.

Acknowledgments

The first author acknowledges INRIA for financial support through the CardioSense3D project. The second author acknowledges the ANR agency for financial support through the PITAC project. We also thank Prof. Erik Burman for the inspiring discussions on Nitsche–based fluid-structure coupling.

A Proof of Lemma 4.5

The main idea consists in adapting, to the non-homogeneous case, a well known property of the Chorin-Temam scheme with a pressure-Poisson equation (see e.g. [3, Page 550]).

From $(35)_1$, we have that

$$\left(\boldsymbol{u}_h^{n+1}-\mathcal{L}_h(D_\tau \boldsymbol{d}_H^{n+1}),\boldsymbol{v}_h^{\mathrm{f}}\right)_{\Omega^{\mathrm{f}}}=\left(\tilde{\boldsymbol{u}}_h^{n}-\mathcal{L}_h(D_\tau \boldsymbol{d}_H^{n+1})-\frac{\tau}{\rho^{\mathrm{f}}}\boldsymbol{\nabla} p_h^{n+1},\boldsymbol{v}_h^{\mathrm{f}}\right)_{\Omega^{\mathrm{f}}}\qquad \forall \boldsymbol{v}_h^{\mathrm{f}}\in V_{\Sigma,h}^{\mathrm{f}}. \tag{49}$$

In addition, thanks to the coupling condition $(35)_2$, it follows that $(\boldsymbol{u}_h^{n+1}-\mathcal{L}_h(D_\tau \boldsymbol{d}_H^{n+1}))\in V_{\Sigma,h}^{\mathrm{f}}$, and therefore (49) reduces to

$$\boldsymbol{u}_h^{n+1}-\mathcal{L}_h(D_\tau \boldsymbol{d}_H^{n+1})=\Pi_h\left(\tilde{\boldsymbol{u}}_h^{n}-\mathcal{L}_h(D_\tau \boldsymbol{d}_H^{n+1})-\frac{\tau}{\rho^{\mathrm{f}}}\boldsymbol{\nabla} p_h^{n+1}\right),$$

or, equivalently,

$$\tilde{\boldsymbol{u}}_h^{n}=\boldsymbol{u}_h^{n+1}+\Pi_h^{\perp}\left(\tilde{\boldsymbol{u}}_h^{n}-\mathcal{L}_h(D_\tau \boldsymbol{d}_H^{n+1})\right)+\frac{\tau}{\rho^{\mathrm{f}}}\Pi_h\left(\boldsymbol{\nabla} p_h^{n+1}\right). \tag{50}$$

On the other hand, integrating by parts in $(34)_1$ and inserting (50) in the resulting expression yields

$$\begin{aligned}
(\boldsymbol{\nabla} p_h^{n+1},\boldsymbol{\nabla} q_h)_{\Omega^{\mathrm{f}}} =&\frac{\rho^{\mathrm{f}}}{\tau}(\tilde{\boldsymbol{u}}_h^{n},\boldsymbol{\nabla} q_h)_{\Omega^{\mathrm{f}}}-\frac{\rho^{\mathrm{f}}}{\tau}(\tilde{\boldsymbol{u}}_h^{n}\cdot\boldsymbol{n}^{\mathrm{f}},q_h)_{\Sigma}-\frac{\rho^{\mathrm{f}}}{\tau}\left((\pi_h(D_\tau \boldsymbol{d}_H^{n+1})-\tilde{\boldsymbol{u}}_h^{n})\cdot\boldsymbol{n}^{\mathrm{f}},q_h\right)_{\Sigma}\\
=&\frac{\rho^{\mathrm{f}}}{\tau}(\tilde{\boldsymbol{u}}_h^{n},\boldsymbol{\nabla} q_h)_{\Omega^{\mathrm{f}}}-\frac{\rho^{\mathrm{f}}}{\tau}(\pi_h(D_\tau \boldsymbol{d}_H^{n+1})\cdot\boldsymbol{n}^{\mathrm{f}},q_h)_{\Sigma}\\
=&\frac{\rho^{\mathrm{f}}}{\tau}(\boldsymbol{u}_h^{n+1},\boldsymbol{\nabla} q_h)_{\Omega^{\mathrm{f}}}+\frac{\rho^{\mathrm{f}}}{\tau}\left(\Pi_h^{\perp}\left(\tilde{\boldsymbol{u}}_h^{n}-\mathcal{L}_h(D_\tau \boldsymbol{d}_H^{n+1})\right),\boldsymbol{\nabla} q_h\right)_{\Omega^{\mathrm{f}}}\\
&+\left(\Pi_h\left(\boldsymbol{\nabla} p_h^{n+1}\right),\boldsymbol{\nabla} q_h\right)_{\Omega^{\mathrm{f}}}-\frac{\rho^{\mathrm{f}}}{\tau}\left(\pi_h(D_\tau \boldsymbol{d}_H^{n+1})\cdot\boldsymbol{n}^{\mathrm{f}},q_h\right)_{\Sigma},
\end{aligned}$$

for all $q_h\in Q_{\Gamma,h}^{\mathrm{f}}$. Finally, reintegrating by parts and using the interface coupling condition $(35)_2$, we get

$$\begin{aligned}
(\boldsymbol{\nabla} p_h^{n+1},\boldsymbol{\nabla} q_h)_{\Omega^{\mathrm{f}}} =&\frac{\rho^{\mathrm{f}}}{\tau}(\boldsymbol{u}_h^{n+1}\cdot\boldsymbol{n}^{\mathrm{f}},q_h)_{\Sigma}-\frac{\rho^{\mathrm{f}}}{\tau}(\boldsymbol{\nabla}\cdot\boldsymbol{u}_h^{n+1},q_h)_{\Omega^{\mathrm{f}}}\\
&+\frac{\rho^{\mathrm{f}}}{\tau}(\Pi_h^{\perp}\left(\tilde{\boldsymbol{u}}_h^{n}-\mathcal{L}_h(D_\tau \boldsymbol{d}_H^{n+1})\right),\boldsymbol{\nabla} q_h)_{\Omega^{\mathrm{f}}}\\
&+\left(\Pi_h\left(\boldsymbol{\nabla} p_h^{n+1}\right),\boldsymbol{\nabla} q_h\right)_{\Omega^{\mathrm{f}}}-\frac{\rho^{\mathrm{f}}}{\tau}\left(\pi_h(D_\tau \boldsymbol{d}_H^{n+1})\cdot\boldsymbol{n}^{\mathrm{f}},q_h\right)_{\Sigma}\\
=&-\frac{\rho^{\mathrm{f}}}{\tau}(\boldsymbol{\nabla}\cdot\boldsymbol{u}_h^{n+1},q_h)_{\Omega^{\mathrm{f}}}+\frac{\rho^{\mathrm{f}}}{\tau}(\Pi_h^{\perp}(\tilde{\boldsymbol{u}}_h^{n}-\mathcal{L}_h(D_\tau \boldsymbol{d}_H^{n+1})),\boldsymbol{\nabla} q_h)_{\Omega^{\mathrm{f}}}\\
&+(\Pi_h(\boldsymbol{\nabla} p_h^{n+1}),\boldsymbol{\nabla} q_h)_{\Omega^{\mathrm{f}}},
\end{aligned}$$

which completes the proof.

References

[1] M. Astorino, F. Chouly, and M.A. Fernández. An added-mass free semi-implicit coupling scheme for fluid-structure interaction. *C. R. Acad. Sci. Paris Sér. I Math.*, 347(1–2):99–104, 2009.

[2] M. Astorino and C. Grandmont. Convergence analysis of a projection semi-implicit coupling scheme for fluid-structure interaction problems. Submitted.

[3] S. Badia and R. Codina. Convergence analysis of the FEM approximation of the first order projection method for incompressible flows with and without the inf-sup condition. *Numer. Math.*, 107:533–557, 2007.

[4] S. Badia, F. Nobile, and C. Vergara. Fluid-structure partitioned procedures based on Robin transmission conditions. *J. Comp. Phys.*, 227:7027–7051, 2008.

[5] S. Badia, A. Quaini, and A. Quarteroni. Splitting methods based on algebraic factorization for fluid-structure interaction. *SIAM J. Sci. Comput.*, 30(4):1778–1805, 2008.

[6] R. Becker, P. Hansbo, and R. Stenberg. A finite element method for domain decomposition with non-matching grids. *M2AN Math. Model. Numer. Anal.*, 37(2):209–225, 2003.

[7] E. Burman and M.A. Fernández. Stabilized explicit coupling for fluid-structure interaction using Nitsche's method. *C. R. Math. Acad. Sci. Paris*, 345(8):467–472, 2007.

[8] E. Burman and M.A. Fernández. Stabilization of explicit coupling in fluid-structure interaction involving fluid incompressibility. *Comput. Methods Appl. Mech. Engrg.*, 198(5–8):766–784, 2009.

[9] P. Causin, J.-F. Gerbeau, and F. Nobile. Added-mass effect in the design of partitioned algorithms for fluid-structure problems. *Comput. Methods Appl. Mech. Engrg.*, 194(42–44):4506–4527, 2005.

[10] A.J. Chorin. On the convergence of discrete approximations to the Navier-Stokes equations. *Math. Comp.*, 23:341–353, 1969.

[11] A. Ern and J.-L. Guermond. *Theory and practice of finite elements*, volume 159 of *Applied Mathematical Sciences*. Springer-Verlag, New York, 2004.

[12] C. Farhat, M. Lesoinne, and P. Le Tallec. Load and motion transfer algorithms for fluid/structure interaction problems with non-matching discrete interfaces: Momentum and energy conservation, optimal discretization and application to aeroelasticity. *Comput. Methods Appl. Mech. Engrg.*, 157:95–114, 1998.

[13] M.A. Fernández, J.-F. Gerbeau, and C. Grandmont. A projection algorithm for fluid-structure interaction problems with strong added-mass effect. *C. R. Math. Acad. Sci. Paris*, 342(4):279–284, 2006.

[14] M.A. Fernández, J.F. Gerbeau, and C. Grandmont. A projection semi-implicit scheme for the coupling of an elastic structure with an incompressible fluid. *Int. J. Num. Meth. Engrg.*, 69(4):794–821, 2007.

[15] M.A. Fernández and M. Moubachir. A Newton method using exact Jacobians for solving fluid-structure coupling. *Comp. & Struct.*, 83:127–142, 2005.

[16] L. Formaggia, J.-F. Gerbeau, F. Nobile, and A. Quarteroni. On the coupling of 3D and 1D Navier-Stokes equations for flow problems in compliant vessels. *Comp. Meth. Appl. Mech. Engrg.*, 191(6-7):561–582, 2001.

[17] L. Formaggia, A. Quarteroni, and A. Veneziani, editors. *Cardiovascular Mathematics. Modeling and simulation of the circulatory system*, volume 1 of *Modeling, Simulation and Applications*. Springer, 2009.

[18] C. Grandmont and Y. Maday. Nonconforming grids for the simulation of fluid-structure interaction. In *Domain decomposition methods, 10 (Boulder, CO, 1997)*, volume 218 of *Contemp. Math.*, pages 262–270. Amer. Math. Soc., Providence, RI, 1998.

[19] J.-L. Guermond. Some implementation of projection methods for Navier-Stokes equations. *M2AN*, 30:637–667, 1996.

[20] J.-L. Guermond and L. Quartapelle. On stability and convergence of projection methods based on pressure Poisson equation. *Internat. J. Numer. Methods Fluids*, 26(9):1039–1053, 1998.

[21] G. Guidoboni, R. Glowinski, N. Cavallini, S. Canic, and S. Lapin. A kinematically coupled time-splitting scheme for fluid-structure interaction in blood flow. *Appl. Math. Lett.*, In Press, 2008. DOI: 10.1016/j.aml.2008.05.006.

[22] P. Hansbo, J. Hermansson, and T. Svedberg. Nitsche's method combined with space-time finite elements for ALE fluid-structure interaction problems. *Comput. Methods Appl. Mech. Engrg.*, 193(39-41):4195–4206, 2004.

[23] F. Hecht, O. Pironneau, A. Le Hyaric, and K. Ohtsuka. *FreeFem++ v. 2.11. User's Manual*. University of Paris 6.

[24] D. P. Mok, W. A. Wall, and E. Ramm. Accelerated iterative substructuring schemes for instationary fluid-structure interaction. In K.J. Bathe, editor, *Computational Fluid and Solid Mechanics*, pages 1325–1328. Elsevier, 2001.

[25] J. Nitsche. Über ein Variationsprinzip zur Lösung von Dirichlet-Problemen bei Verwendung von Teilräumen, die keinen Randbedingungen unterworfen sind. *Abh. Math. Sem. Univ. Hamburg*, 36:9–15, 1971.

[26] F. Nobile and C. Vergara. An effective fluid-structure interaction formulation for vascular dynamics by generalized Robin conditions. *SIAM J. Sci. Comput.*, 30(2):731–763, 2008.

[27] A. Quaini and A. Quarteroni. A semi-implicit approach for fluid-structure interaction based on an algebraic fractional step method. *Math. Models Methods Appl. Sci.*, 17(6):957–983, 2007.

[28] A.-V. Salsac, M.A. Fernández, J.M. Chomaz, and P. Le Tallec. Effects of the flexibility of the arterial wall on the wall shear stresses and wall tension in abdominal aortic aneurysms. In *Bulletin of the American Physical Society*, 2005.

[29] A.-V. Salsac, S.R. Sparks, J.M. Chomaz, and J.C. Lasheras. Evolution of the wall shear stresses during the progressive enlargement of symmetric abdominal aortic aneurysms. *J. Fluid Mech.*, 550:19–51, 2006.

[30] S. Soyibou and C.M. Murea. A stable time advancing scheme for solving fluid-structure interaction problem at small structural displacements. *Comput. Methods Appl. Mech. Engrg.*, 198(2):210 – 222, 2008.

[31] R. Temam. Une méthode d'approximation de la solution des équations de Navier-Stokes. *Bull. Soc. Math. France*, 96:115–152, 1968.

[32] V. Thomée. *Galerkin finite element methods for parabolic problems*, volume 25 of *Springer Series in Computational Mathematics*. Springer-Verlag, Berlin, second edition, 2006.

[33] L. Tobiska and R. Verfürth. Analysis of a streamline diffusion finite element method for the Stokes and Navier-Stokes equations. *SIAM J. Numer. Anal.*, 33(1):107–127, 1996.

Contents

1 Introduction **3**

2 Preliminaries **4**
2.1 The Coupled Problem 4
2.2 Time Semi-Discretization 5

3 Robin Based Semi-Implicit Coupling **6**
3.1 Notation 6
3.2 The Coupling Scheme 7
3.3 Pressure Load Computation 9
3.4 Variants 10
3.4.1 Pressure-Poisson Formulation 10
3.4.2 Pressure-Correction Formulation 11

4 Stability Analysis **11**
4.1 A Simplified Model Problem 11
4.2 Semi-Implicit Coupling With Pressure-Darcy Formulation 12
4.2.1 Energy Based Stability Analysis 13
4.3 Semi-Implicit Coupling With Pressure-Poisson Formulation . . . 15
4.3.1 Energy Based Stability Analysis 16

5 Numerical Experiments **18**
5.1 Two-Dimensional Test-Cases 19
5.1.1 An Analytical Test-Case 19
5.1.2 Pressure Wave Propagation in a Compliant Vessel 20
5.2 Three-Dimensional Test-Cases 20
5.2.1 Pressure Wave Progation in a Straight Cylindrical Vessel 21
5.2.2 A Physiological Test-Case 21

6 Conclusion **24**

A Proof of Lemma 4.5 **26**

Unité de recherche INRIA Rocquencourt
Domaine de Voluceau - Rocquencourt - BP 105 - 78153 Le Chesnay Cedex (France)

Unité de recherche INRIA Futurs : Parc Club Orsay Université - ZAC des Vignes
4, rue Jacques Monod - 91893 ORSAY Cedex (France)
Unité de recherche INRIA Lorraine : LORIA, Technopôle de Nancy-Brabois - Campus scientifique
615, rue du Jardin Botanique - BP 101 - 54602 Villers-lès-Nancy Cedex (France)
Unité de recherche INRIA Rennes : IRISA, Campus universitaire de Beaulieu - 35042 Rennes Cedex (France)
Unité de recherche INRIA Rhône-Alpes : 655, avenue de l'Europe - 38334 Montbonnot Saint-Ismier (France)
Unité de recherche INRIA Sophia Antipolis : 2004, route des Lucioles - BP 93 - 06902 Sophia Antipolis Cedex (France)

Éditeur
INRIA - Domaine de Voluceau - Rocquencourt, BP 105 - 78153 Le Chesnay Cedex (France)
http://www.inria.fr
ISSN 0249-6399